Supplementary Information for

Highly planar diarylamine-fused porphyrins and their remarkably stable radical cations

Norihito Fukui,[a] Wonhee Cha,[b] Daiki Shimizu,[a] Juwon Oh,[b] Ko Furukawa,[c] Hideki Yorimitsu,[a] Dongho Kim,[b] and Atsuhiro Osuka[a]

[a]Department of Chemistry, Graduate School of Science, Kyoto University, Sakyo-ku, Kyoto 606-8502, Japan.

[b]Spectroscopy Laboratory of Functional π-Electronic Systems and Department of Chemistry, Yonsei University, Seoul 120-749, Korea.

[c]Center for Instrumental Analysis, Niigata University, Nishi-ku, Niigata 950-2181, Japan.

Contents

1. Instrumentation and Materials

^{1}H NMR (600 MHz) and ^{13}C NMR (151 MHz) spectra were taken on a JEOL ECA-600 spectrometer. Chemical shifts were reported as delta scale in ppm relative to $CHCl_3$ (δ = 7.26) for ^{1}H NMR and to $CDCl_3$ (δ = 77.16) for ^{13}C NMR. UV/Vis absorption spectra were recorded on a Shimadzu UV-3600 spectrometer. High-resolution APCI-TOF mass spectra were taken on a Bruker micrOTOF. X-Ray data were taken at –180 °C with a Rigaku XtaLAB P200 diffractometer by using graphite monochromated Cu-K_α radiation (λ = 1.54187 Å). The structures were solved by direct method SIR-97 and refined by SHELXL-97 program.[S1] Preparative separations were performed by silica gel column chromatography (Wako gel C-200, C-300, and C-400). Toluene was distilled from CaH_2. THF was purified by passing through a neutral alumina column under N_2. $CHCl_3$ was purified by passing through an alumina column. Unless otherwise noted, materials obtained from commercial suppliers were used without further purification. Palau'Chlor was purchased from Sigma-Aldrich.

2. Experimental Procedures

Singly phenoxazine-fused Ni(II) porphyrin 9. A flask containing *meso*-phenoxazino Ni(II) porphyrin **7** (111 mg, 100 μmol), DDQ (227 mg, 1.0 mmol), and $Sc(OTf)_3$ (492 mg, 1.0 mmol) was purged with argon, and then charged with $ClCH_2CH_2Cl$ (17.5 mL) and $MeNO_2$ (17.5 mL). The mixture was stirred at 70 °C for 1 h. The reaction was quenched by addition of a saturated aqueous $NaHCO_3$ solution. The organic phase was separated and washed with water and brine, and dried over anhydrous Na_2SO_4. After removal of the solvent *in vacuo*, the reaction mixture was diluted with THF and filtered through a small plug of alumina with copious washings (THF). After removal of the solvent *in vacuo*, the residue was separated by silica gel chromatography eluting with CH_2Cl_2/hexane. Recrystallization from CH_2Cl_2/MeOH gave **9** (63.9 mg, 57.5 μmol, 58%). ^1H NMR (600 MHz, $CDCl_3$, 60 °C): δ = 9.16 (d, J = 4.6 Hz, 1H, β), 8.97 (s, 1H, β), 8.68 (d, J = 4.6 Hz, 1H, β), 8.66 (d, J = 4.6 Hz, 1H, β), 8.63 (d, J = 4.6 Hz, 1H, β), 8.60 (d, J = 4.6 Hz, 1H, β), 8.52 (d, J = 4.6 Hz, 1H, β), 8.17 (d, J = 7.8 Hz, 1H, phenoxazine), 7.79 (t, J = 1.8 Hz, 1H, Ar), 7.72 (t, J = 1.8 Hz, 1H, Ar), 7.71 (t, J = 1.8 Hz, 1H, Ar), 7.47 (t, J = 7.8 Hz, 1H, phenoxazine), 7.31 (d, J = 7.8 Hz, 1H, phenoxazine), 7.21 (d, J = 7.8 Hz, 1H, phenoxazine), 7.03 (t, J = 7.8 Hz, 1H, phenoxazine), 7.00 (d, J = 7.8 Hz, 1H, phenoxazine), 6.59 (t, J = 7.8 Hz, 1H, phenoxazine), and 1.60-1.30 (m, 54H, *tert*-butyl) ppm (The signals for the some protons of the 3,5-di-*tert*-butylphenyl groups are too broad to analyze because of flapping of the porphyrin skeleton and/or rotation of the 3,5-di-*tert*-butylphenyl groups.); ^{13}C NMR (151 MHz, $CDCl_3$, 60 °C): δ = 149.74, 149.41, 149.34, 148.40, 147.85, 144.40, 143.80, 143.21, 142.94, 141.33, 140.26, 140.11, 139.83, 139.78, 134.88, 134.76, 134.48, 133.83, 133.13, 132.90, 132.60, 131.58, 131.25, 128.75, 128.71, 128.63 (overlap), 127.57, 126.01, 124.58, 123.57, 121.39, 121.34, 121.20, 121.13 (overlap), 119.19, 119.07, 117.99, 117.35, 116.10, 115.34, 114.89, 114.40, 35.25, 35.18 (overlap), 31.91, and 31.87 (overlap) ppm; APCI-TOF-MS: m/z = 1109.5472. Calcd for $C_{74}H_{77}N_5{}^{58}NiO$: 1109.5487 $[M]^-$; UV/Vis (CH_2Cl_2): λ_{max} (ε [$M^{-1}cm^{-1}$]) = 393 (4.10×10^4), 462 (1.48×10^5), and 621 nm (2.52×10^4).

Doubly phenoxazine-fused Ni(II) porphyrin 4Ni. A flask containing **9** (11.1 mg, 10 μmol) was purged with argon, and then charged with $ClCH_2CH_2Cl$ (3.0 mL) and $FeCl_3$ (16.2 mg, 100 μmol) dissolved in $MeNO_2$ (0.5 mL). The mixture was stirred at 90 °C for 1 h. The reaction was quenched by addition of a saturated aqueous $NaHCO_3$ solution. The organic phase was separated and washed with water and brine, and dried over anhydrous Na_2SO_4. After removal of the solvent *in vacuo*, the reaction mixture was diluted with THF and filtered through a small plug of alumina with copious washings (THF). After removal of the solvent *in vacuo*, the residue was passed through a small plug of silica gel with copious washings ($CHCl_3$). After removal of the solvent *in vacuo*, a flask containing the residue, $Pd_2(dba)_3$ (9.2 mg, 10 μmol), and SPhos (8.2 mg, 20 μmol) was purged with argon, and then charged with toluene (1.0 mL), NEt_3 (14 μL, 100 μmol), and HCOOH (4 μL, 100 μmol). The mixture was stirred at 120 °C for 1 h. The reaction mixture was diluted with CH_2Cl_2 and filtered through a small plug of Celite® with copious washings (CH_2Cl_2). After removal of the solvent *in vacuo*, the residue was separated by silica gel chromatography eluting with CH_2Cl_2/hexane. Recrystallization from CH_2Cl_2/MeOH gave **4Ni** (6.4 mg, 5.8 μmol, 58%). ^1H NMR (600 MHz, $CDCl_3$, 25 °C, 10 mM): δ = 8.91 (s, 2H, β), 8.76 (d, J = 4.8 Hz, 2H, β), 8.71 (d, J = 4.8 Hz, 2H, β), 8.05 (d, J = 1.9 Hz, 2H,

Ar), 8.02 (d, J = 1.9 Hz, 4H, Ar), 8.00 (d, J = 6.9 Hz, 2H, phenoxazine), 8.12 (t, J = 1.9 Hz, 2H, Ar), 7.75 (t, J = 1.9 Hz, 1H, Ar), 7.21 (t, J = 6.9 Hz, 2H, phenoxazine), 6.51 (d, J = 6.9 Hz, 2H, phenoxazine), 1.58 (s, 36H, *tert*-butyl), and 1.54 (s, 18H, *tert*-butyl) ppm; ^{13}C NMR (151 MHz, $CDCl_3$, 25 °C, 10 mM): δ = 149.30, 149.11, 146.34, 144.54, 142.36, 141.80, 141.33, 141.16, 133.52, 130.98, 129.06, 128.82, 127.71, 127.02, 125.25, 121.10, 120.76, 120.18, 120.12, 119.34, 117.80, 114.43, 114.40, 113.66, 111.72, 35.27, 35.21, 32.00, and 31.95 ppm; APCI-TOF-MS: m/z = 1107.5294. Calcd for $C_{74}H_{75}N_5{}^{58}NiO$: 1107.5331 [M]$^-$; UV/Vis ($CH_2Cl_2$): λ_{max} (ε [$M^{-1}cm^{-1}$]) = 447 (1.62 × 10^5), 570 (1.27 × 10^4), and 614 nm (3.33 × 10^4).

Doubly phenoxazine-fused free base porphyrin 4H$_2$. Conc. H_2SO_4 (1.0 mL) was added slowly to a mixture of **4Ni** (23.9 mg, 21.5 μmol) and TFA (2.0 mL) at 0 °C. The reaction mixture was stirred at 0 °C in air for 1.5 h, and then poured into water at 0 °C. After neutralization with NaOH and Na_2CO_3 at 0 °C, the product was extracted with CH_2Cl_2, and the organic extract was washed with brine, and dried over anhydrous Na_2SO_4. After removal of the solvent *in vacuo*, the residue was separated by silica gel chromatography eluting with CH_2Cl_2/hexane. Recrystallization of the separated solids from CH_2Cl_2/MeOH gave **4H$_2$** (9.5 mg, 9.0 μmol, 42%). ^{1}H NMR (600 MHz, $CDCl_3$, 25 °C, 5.0 mM): δ = 9.18 (s, 2H, β), 8.77 (d, J = 4.6 Hz, 2H, β), 8.64 (d, J = 4.6 Hz, 2H, β), 8.40 (d, J = 6.9 Hz, 2H, phenoxazine), 8.19 (d, J = 1.9 Hz, 4H, Ar), 8.07 (d, J = 1.9 Hz, 2H, Ar), 7.86 (t, J = 1.9 Hz, 2H, Ar), 7.76 (t, J = 1.9 Hz, 1H, Ar), 7.58 (t, J = 6.9 Hz, 2H, phenoxazine), 7.13 (d, J = 6.9 Hz, 2H, phenoxazine), 1.60 (s, 36H, *tert*-butyl), 1.54 (s, 18H, *tert*-butyl), and –0.53 (br s, 2H, inner NH) ppm; ^{13}C NMR (151 MHz, $CDCl_3$, 25 °C, 5.0 mM): δ = 149.37, 148.93, 145.45, 142.07, 141.57, 129.67, 129.51, 126.32, 121.38, 121.32, 121.17, 120.66, 120.56, 118.92, 114.96, 114.31, 113.09, 112.54, 35.31, 35.18, and 31.99 (overlap) ppm (The signals for the carbons of the porphyrin skeleton were too broad to analyze because of exchange of the inner NH protons.); APCI-TOF-MS: m/z = 1051.6089. Calcd for $C_{74}H_{77}N_5O$: 1051.6134 [M]$^-$; UV/Vis (CH_2Cl_2): λ_{max} (ε [$M^{-1}cm^{-1}$]) = 367 (3.31 × 10^4), 452 (1.56 × 10^5), 549 (8.56 × 10^3), 591 (2.23 × 10^4), 620 (1.29 × 10^5), and 680 nm (3.74 × 10^4); Fluorescence (CH_2Cl_2, λ_{ex} = 452 nm): λ_{max} = 686 and 755 nm, Φ_F = 24.3%.

Doubly phenoxazine-fused Zn(II) porphyrin 4Zn. 4H$_2$ (7.5 mg, 7.1 μmol) was dissolved in CH_2Cl_2 (5 mL). After addition of an excess amount of $Zn(OAc)_2{\cdot}2H_2O$ (10 mg, 46 μmol) dissolved in MeOH (1 mL), the mixture was stirred for 1.5 h at room temperature with shielded from the light in air. The residue was passed through a small plug of silica-gel with copious washings (CH_2Cl_2). After removal of the solvent *in vacuo*, the residue was separated by silica gel chromatography eluting with CH_2Cl_2/hexane. Recrystallization of the separated solids from CH_2Cl_2/MeOH gave **4Zn** (4.5 mg, 4.0 μmol, 57%). ^{1}H NMR (600 MHz, $CDCl_3$, 25 °C, 1.5 mM): δ = 9.29 (s, 2H, β), 8.91 (d, J = 4.6 Hz, 2H, β), 8.78 (d, J = 4.6 Hz, 2H, β), 8.44 (d, J = 7.8 Hz, 2H, phenoxazine), 8.20 (d, J = 1.4 Hz, 4H, Ar), 8.04 (d, J = 1.4 Hz, 2H, Ar), 7.86 (t, J = 1.4 Hz, 2H, Ar), 7.74 (t, J = 1.6 Hz, 1H, Ar), 7.57 (t, J = 7.8 Hz, 2H, phenoxazine), 7.13 (d, J = 7.8 Hz, 2H, phenoxazine), 1.59 (s, 36H, *tert*-butyl), and 1.52 (s, 18H, *tert*-butyl) ppm; ^{13}C NMR (151 MHz, $CDCl_3$, 25 °C, 5.0 mM): δ =154.13, 149.43, 149.17, 149.04, 148.84, 145.07, 142.41, 142.35, 133.71, 133.57, 131.42, 129.77,

129.41, 128.18, 125.92, 122.55, 121.49, 120.96, 120.50, 120.20, 118.95, 115.54, 115.50, 114.25, 111.98, 35.31, 35.19, 32.01, and 31.68; APCI-TOF-MS: *m*/*z* = 1113.5233. Calcd for $C_{74}H_{75}N_5{}^{64}ZnO$: 1113.5269 $[M]^-$; UV/Vis (CH_2Cl_2): λ_{max} (ε [$M^{-1}cm^{-1}$]) = 436 (9.88×10^4), 450 (2.71×10^5), 591 (1.27×10^4), and 640 nm (3.75×10^4); Fluorescence (CH_2Cl_2, λ_{ex} = 452 nm): λ_{max} = 648 and 706 nm, Φ_F = 15.7%.

Doubly diphenylamine-fused free base porphyrin 10H$_2$. 10Ni (21.9 mg, 20 μmol) was placed in a Schlenk flask. The flask was filled with argon. Toluene (1.0 mL) was added to the flask. To the solution, 4-methylphenylmagnesium bromide (0.26 mL, 0.2 mmol, 0.66 M THF solution) was then added. The mixture was stirred at room remperature for 1.5 h. The reaction was quenched with 3 M HCl aq. and extracted with CH_2Cl_2 three times. The combined organic layer was washed with a saturated aqueous $NaHCO_3$ solution and brine and then dried over anhydrous Na_2SO_4. After removal of the solvent *in vacuo*, the residue was separated by silica gel chromatography eluting with CH_2Cl_2/hexane. Recrystallization of the separated solids from CH_2Cl_2/MeOH gave **10H$_2$** (11.7 mg, 11.3 μmol, 56%). ^{1}H NMR (600 MHz, $CDCl_3$, 25 °C): δ = 9.38 (s, 2H, β), 9.07 (d, *J* = 8.7 Hz, 2H, diphenylamine), 9.02 (d, *J* = 8.7 Hz, 2H, diphenylamine), 8.84 (d, *J* = 4.6 Hz, 2H, β), 8.68 (d, *J* = 4.6 Hz, 2H, β), 8.32-8.10 (br d, *J* = 518 Hz, 4H, Ar), 8.04 (d, *J* = 1.9 Hz, 2H, Ar), 7.88 (t, *J* = 1.9 Hz, 2H, Ar), 7.83 (t, *J* = 8.7 Hz, 2H, diphenylamine), 7.76-7.70 (m, 3H, Ar + diphenylamine), 1.61 (br s, 36H, *tert*-butyl), 1.52 (s, 18H, *tert*-butyl), and –0.58 (br s, 2H, inner NH) ppm; ^{13}C NMR (151 MHz, $CDCl_3$, 25 °C): δ = 149.40, 148.87, 142.05, 141.51, 134.82, 132.22, 131.03, 129.85, 129.67, 126.00, 125.52, 125.24, 123.91, 123.69, 121.72, 121.19, 120.70, 118.65, 114.99, 113.74, 35.31, 35.16, and 31.96 (overlap) ppm (The signals for the carbons of the porphyrin skeleton were too broad to analyze because of exchange of the inner NH protons.); APCI-TOF-MS: *m*/*z* = 1037.6308. Calcd for $C_{74}H_{79}N_5$: 1037.6341 $[M]^-$; UV/Vis (CH_2Cl_2): λ_{max} (ε [$M^{-1}cm^{-1}$]) = 440 (1.79×10^5), 453 (1.79×10^5), 551 (9.66×10^3), 593 (2.65×10^4), 618 (1.20×10^4), and 678 nm (3.52×10^4); Fluorescence (CH_2Cl_2, λ_{ex} = 452 nm): λ_{max} = 683 and 750 nm, Φ_F = 16.8%.

Doubly diphenylamine-fused Zn(II) porphyrin 10Zn. 10H$_2$ (19.4 mg, 18.7 μmol) was dissolved in CH_2Cl_2 (30 mL). After addition of an excess amount of $Zn(OAc)_2{\cdot}2H_2O$ (22.5 mg, 0.10 mmol) dissolved in MeOH (1.0 mL), the mixture was stirred for 1.5 h at room temperature with shielded from the light in air. The residue was passed through a small plug of silica-gel with copious washings (CH_2Cl_2). After removal of the solvent *in vacuo*, the residue was separated by silica gel chromatography eluting with CH_2Cl_2/hexane. Recrystallization of the separated solids from CH_2Cl_2/hexane gave **10Zn** (13.7 mg, 12.4 μmol, 67%). ^{1}H NMR (600 MHz, $CDCl_3$, 25 °C): δ = 9.45 (s, 2H, β), 9.10 (d, *J* = 8.3 Hz, 2H, diphenylamine), 9.04 (d, *J* = 8.3 Hz, 2H, diphenylamine), 8.95 (d, *J* = 4.6 Hz, 2H, β), 8.81 (d, *J* = 4.6 Hz, 2H, β), 8.32-8.10 (br d, *J* = 866 Hz, 4H, Ar), 8.05 (d, *J* = 1.8 Hz, 2H, Ar), 7.88 (t, *J* = 1.8 Hz, 2H, Ar), 7.83 (t, *J* = 8.3 Hz, 2H, diphenylamine), 7.76-7.70 (m, 3H, Ar + diphenylamine), 1.61 (br s, 36H, *tert*-butyl), and 1.53 (s, 18H, *tert*-butyl) ppm; ^{13}C NMR (151 MHz, $CDCl_3$, 25 °C): δ = 153.68, 150.15, 149.18, 149.09, 148.79, 142.35, 142.26, 135.49, 134.76, 133.50, 131.45, 130.41, 129.71, 129.54, 126.13, 125.30, 125.10, 123.94, 123.83, 122.90, 120.99, 120.52, 119.32, 116.23, 114.92, 35.31, 35.17, and 31.98 (overlap) ppm; APCI-TOF-MS: *m*/*z* = 1099.5463. Calcd for $C_{74}H_{77}N_5{}^{64}Zn$:

1099.5476 [M]$^{-}$; UV/Vis (CH_2Cl_2): λ_{max} (ε [$M^{-1}cm^{-1}$]) = 439 (2.31 × 10^5), 453 (3.68 × 10^5), 585 (1.58 × 10^3), and 632 nm (4.66 × 10^4); Fluorescence (CH_2Cl_2, λ_{ex} = 452 nm): λ_{max} = 640 and 695 nm, Φ_F = 12.9%.

***β*-Dichloro phenoxazine-fused Ni(II) porphyrin 13. 4Ni** (22.2 mg, 20 μmol) was dissolved in $CHCl_3$ (12 mL). The mixture was stirred at 0 °C, and Palau'Chlor (2.0 mL, 44 μmol, 22 mM $CHCl_3$ solution) was added dropwise over 10 min. Then, the mixture was stirred at room temperature for 2.5 h. The reaction mixture was diluted with CH_2Cl_2 and filtered through a small plug of silica gel with copious washings (CH_2Cl_2). After removal of the solvent *in vacuo*, recrystallization from $CHCl_3$/MeOH gave **13** (18.2 mg, 15.4 μmol, 77%). ^{1}H NMR (600 MHz, $CDCl_3$, 25 °C, 1.6 mM): δ = 9.12 (d, *J* = 6.8 Hz, 2H, phenoxazine), 8.86 (d, *J* = 5.0 Hz, 2H, *β*), 8.60 (d, *J* = 5.0 Hz, 2H, *β*), 7.82 (d, *J* = 1.9 Hz, 2H, Ar), 7.72-7.68 (m, 5H, Ar), 7.67 (t, *J* = 1.9 Hz, 2H, Ar), 7.41 (t, *J* = 6.8 Hz, 2H, phenoxazine), 6.96 (d, *J* = 6.8 Hz, 2H, phenoxazine), and 1.46 (br s, 54H, *tert*-butyl) ppm; The ^{13}C NMR signals were too weak to analyze because of the low solubility.; APCI-TOF-MS: *m*/*z* = 1175.4510. Calcd for $C_{74}H_{73}N_5{}^{58}NiO^{35}Cl_2$: 1175.4551 [M]$^{-}$; UV/Vis ($CH_2Cl_2$): λ_{max} (ε [$M^{-1}cm^{-1}$]) = 402 (4.37 × 10^4), 455 (1.68 × 10^5), 598 (1.46 × 10^4), and 628 nm (2.94 × 10^4).

***β*-Dichloro phenoxazine-fused Ni(II) porphyrinium hexachloroantimonate [13]$^+$. 13** (9.4 mg, 8.0 μmol) was dissolved in CH_2Cl_2 (20 mL). The mixture was stirred at room temperature, and tris(4-bromophenyl)aminium hexachloroantimonate (10 mL, 8.8 μmol, 0.88 mM CH_2Cl_2 solution) was added to the mixture. Then, the mixture was stirred at room temperature in air for 10 min. The reaction mixture was diluted with CH_2Cl_2 and filtered through a small plug of silica gel with copious washings (CH_2Cl_2). After removal of the solvent *in vacuo*, recrystallization from CH_2Cl_2/hexane gave **[13]$^+$** (9.5 mg, 6.3 μmol, 79%). ^{1}H NMR (600 MHz, $CDCl_3$, 25 °C): δ = 1.64 (br s, 18H, *tert*-butyl) and 1.58 (br s, 36H, *tert*-butyl) ppm; UV/Vis (CH_2Cl_2): λ_{max} (ε [$M^{-1}cm^{-1}$]) = 403 (5.34 × 10^4), 467 (7.01 × 10^4), 543 (1.93 × 10^4), 609 (1.19 × 10^4), 677 (1.19 × 10^4), 1092 nm (1.11 × 10^4), and 1583 nm (7.05 × 10^2).

***β*-Dichloro diphenylamine-fused porphyrin 14. 10Ni** (11.0 mg, 10 μmol) was dissolved in $CHCl_3$ (2.0 mL). The mixture was stirred at 0 °C, and Palau'Chlor (0.5 mL, 21 μmol, 42 mM $CHCl_3$ solution) was added dropwise over 10 min. Then, the mixture was stirred at room temperature for 7 h. The reaction mixture was diluted with CH_2Cl_2 and filtered through a small plug of silica gel with copious washings (CH_2Cl_2). After removal of the solvent *in vacuo*, recrystallization from CH_2Cl_2/MeOH gave **14** (10.1 mg, 8.7 μmol, 87%). ^{1}H NMR (600 MHz, $CDCl_3$, 25 °C): δ = 9.63 (d, *J* = 7.8 Hz, 2H, diphenylamine), 8.81 (d, *J* = 5.0 Hz, 2H, *β*), 8.74 (d, *J* = 7.8 Hz, 2H, diphenylamine), 8.61 (d, *J* = 5.0 Hz, 2H, *β*), 7.86 (d, *J* = 1.9 Hz, 2H, Ar), 7.75 (t, *J* = 1.9 Hz, 2H, Ar), 7.70 (t, *J* = 1.9 Hz, 1H, Ar), 7.68 (t, *J* = 7.8 Hz, 2H, diphenylamine), 7.62 (t, *J* = 7.8 Hz, 2H, diphenylamine), 1.50 (br s, 36H, *tert*-butyl), and 1.48 (s, 18H, *tert*-butyl) ppm (The signals for the some protons of the 3,5-di-*tert*-butylphenyl groups are too broad to analyze because of flapping of the porphyrin skeleton.); ^{13}C NMR (151 MHz, $CDCl_3$, 25 °C): δ = 149.33, 149.27, 146.05, 143.48, 140.07, 139.08, 137.60, 134.33, 133.14, 131.07, 128.84, 128.34, 126.65, 126.48, 126.24, 124.71 (overlap), 122.97, 122.31, 121.14, 121.10,

119.33, 117.98, 116.19, 115.78, 35.18, 35.15, and 31.85 (overlap); APCI-TOF-MS: *m*/*z* = 1161.4719. Calcd for $C_{74}H_{75}N_5{}^{58}Ni^{35}Cl_2$: 1161.4758 $[M]^-$; UV/Vis (CH_2Cl_2): λ_{max} (ε [$M^{-1}cm^{-1}$]) = 453 (1.86×10^5), 570 (1.40×10^5), and 615 nm (3.27×10^4).

***β*-Dichloro diphenylamine-fused Ni(II) porphyrinium hexachloroantimonate [14]$^+$. 14** (17.5 mg, 15.0 μmol) was dissolved in CH_2Cl_2 (10 mL). The mixture was stirred at room temperature, and tris(4-bromophenyl)aminium hexachloroantimonate (13.5 mg, 16.5 μmol) was added to the mixture. Then, the mixture was stirred at room temperature in air for 5 min. The reaction mixture was diluted with CH_2Cl_2 and filtered through a small plug of silica gel with copious washings (CH_2Cl_2). After removal of the solvent *in vacuo*, recrystallization from CH_2Cl_2/hexane gave **[14]**$^+$ (20.5 mg, 13.7 μmol, 91%). ^1H NMR (600 MHz, $CDCl_3$, 25 °C): δ = 1.61 (br s, 18H, *tert*-butyl) and 1.57 (br s, 36H, *tert*-butyl) ppm; UV/Vis (CH_2Cl_2): λ_{max} (ε [$M^{-1}cm^{-1}$]) = 441 (7.19×10^4), 460 (8.00×10^4), 543 (2.26×10^4), 663 (1.45×10^4), and 903 nm (8.89×10^3).

3. Compound Data

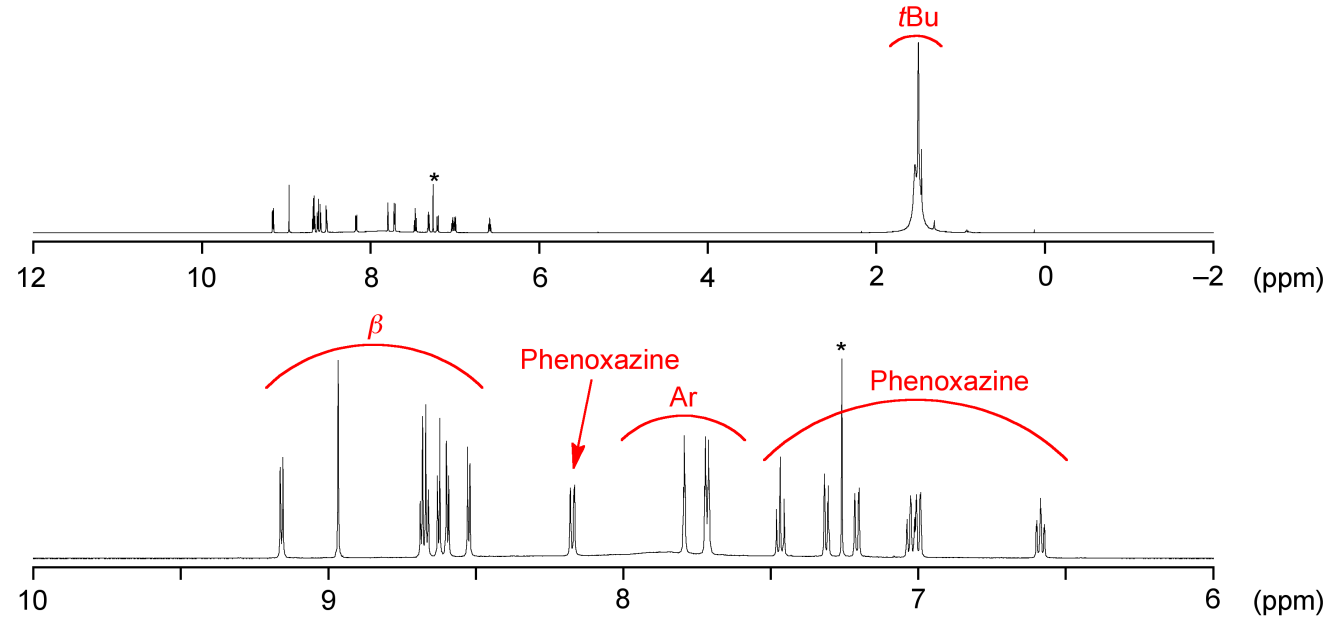

Figure S 1. ^{1}H NMR spectrum of **9** in $CDCl_3$ at 60 °C. *Solvent.

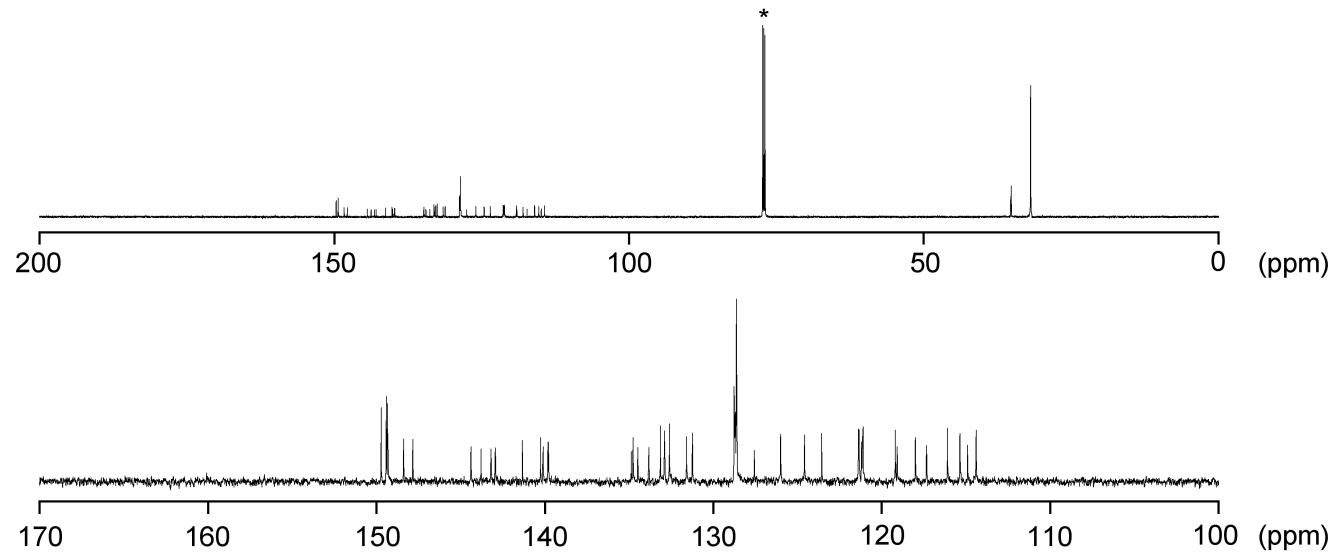

Figure S 2. ^{13}C NMR spectrum of **9** in $CDCl_3$ at 60 °C. *Solvent.

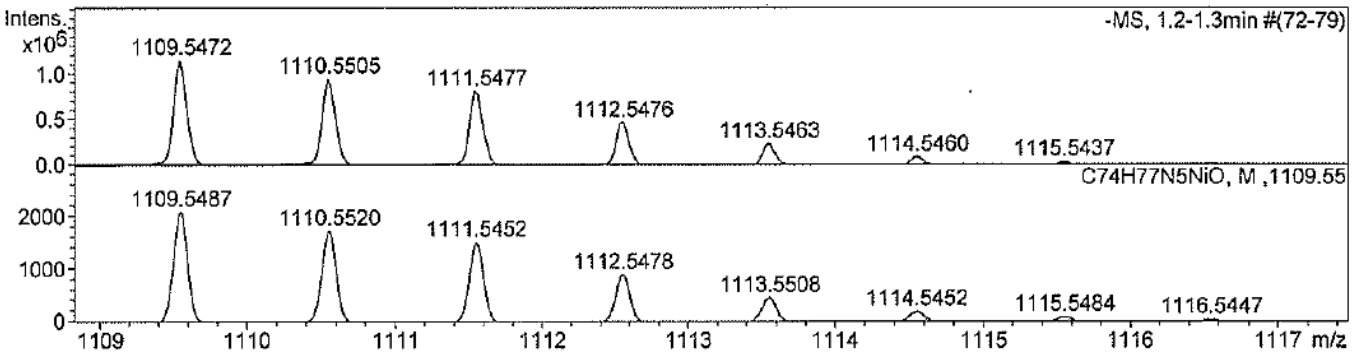

Figure S 3. Observed (top) and simulated (bottom) HR-APCI-TOF MS of **9**.

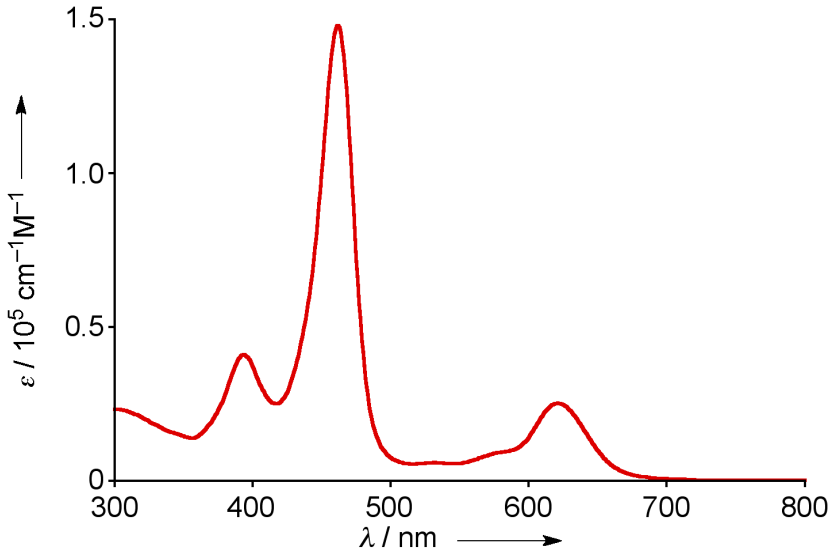

Figure S 4. UV/Vis absorption spectrum of **9** in CH_2Cl_2.

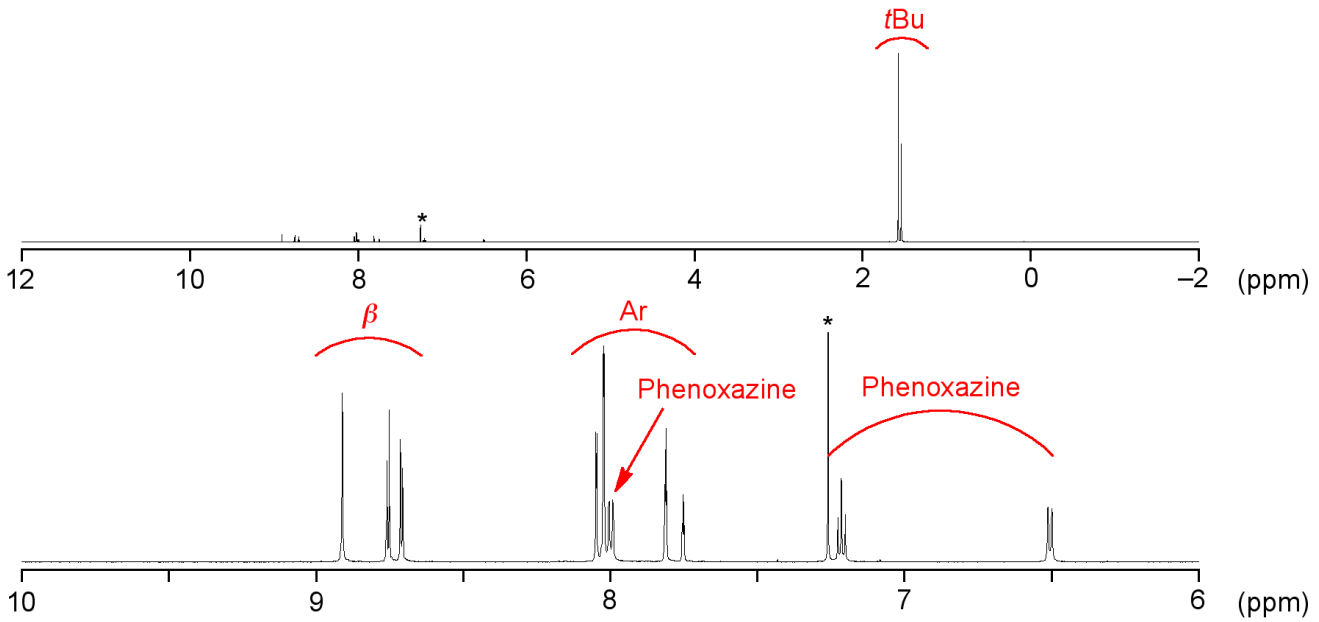

Figure S 5. ^{1}H NMR spectrum of **4Ni** in $CDCl_3$ at 25 °C. *Solvent.

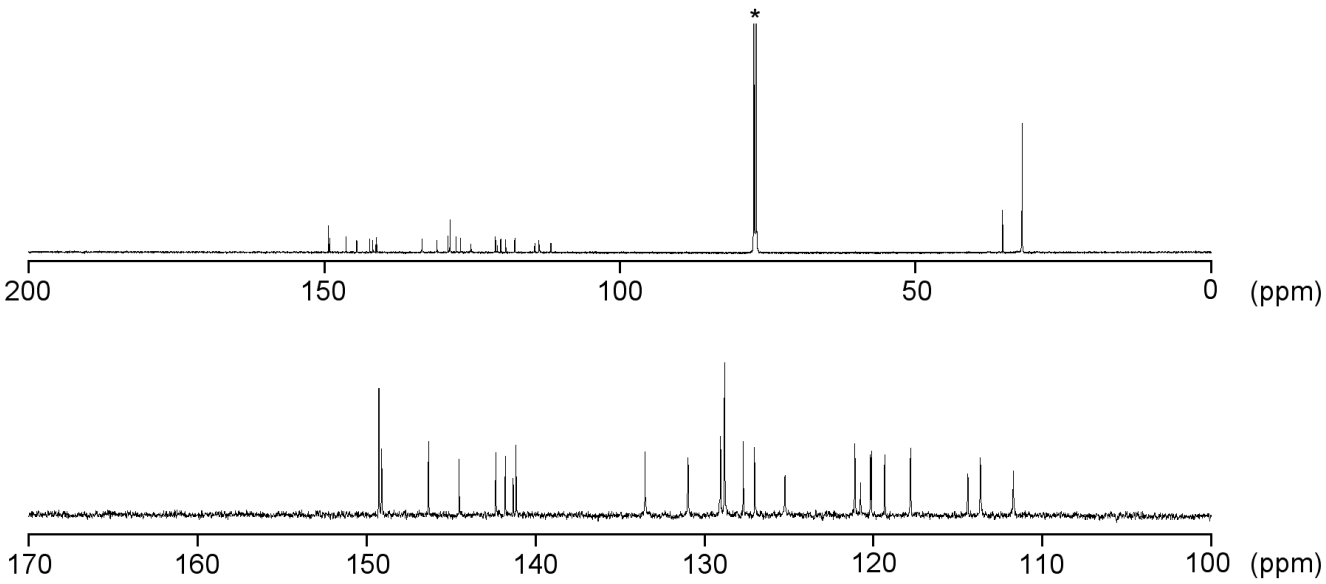

Figure S 6. ^{13}C NMR spectrum of **4Ni** in $CDCl_3$ at 25 °C. *Solvent.

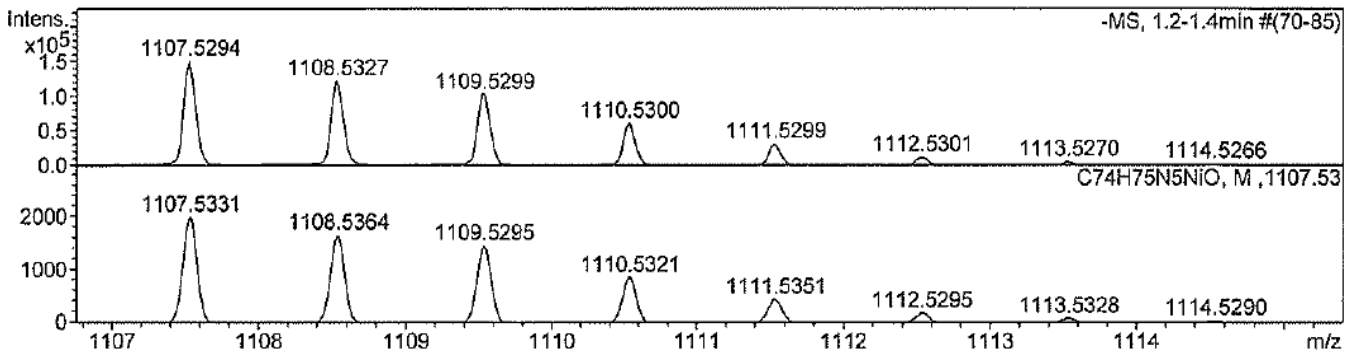

Figure S 7. Observed (top) and simulated (bottom) HR-APCI-TOF MS of **4Ni**.

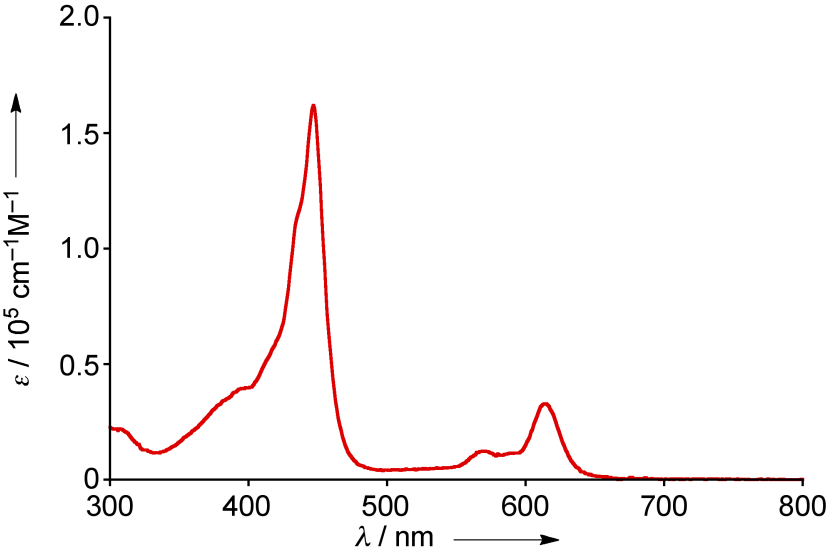

Figure S 8. UV/Vis absorption spectrum of **4Ni** in CH_2Cl_2.

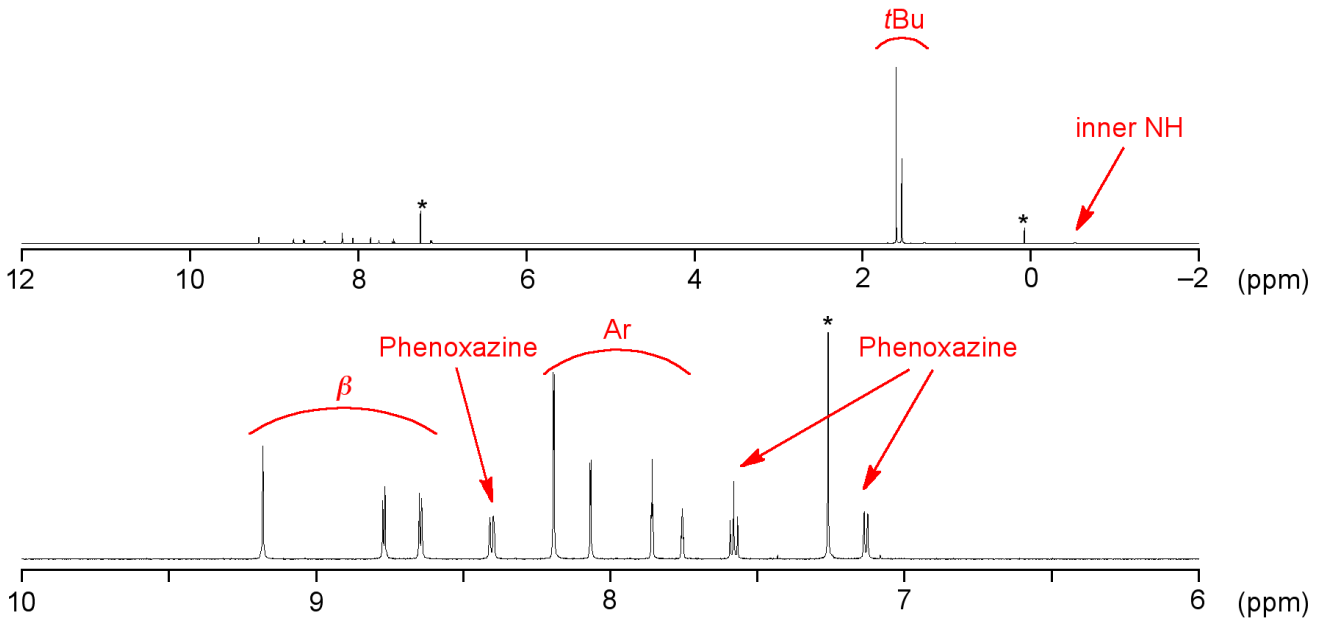

Figure S 9. ^{1}H NMR spectrum of **4H$_2$** in $CDCl_3$ at 25 °C. *Solvent and impurities.

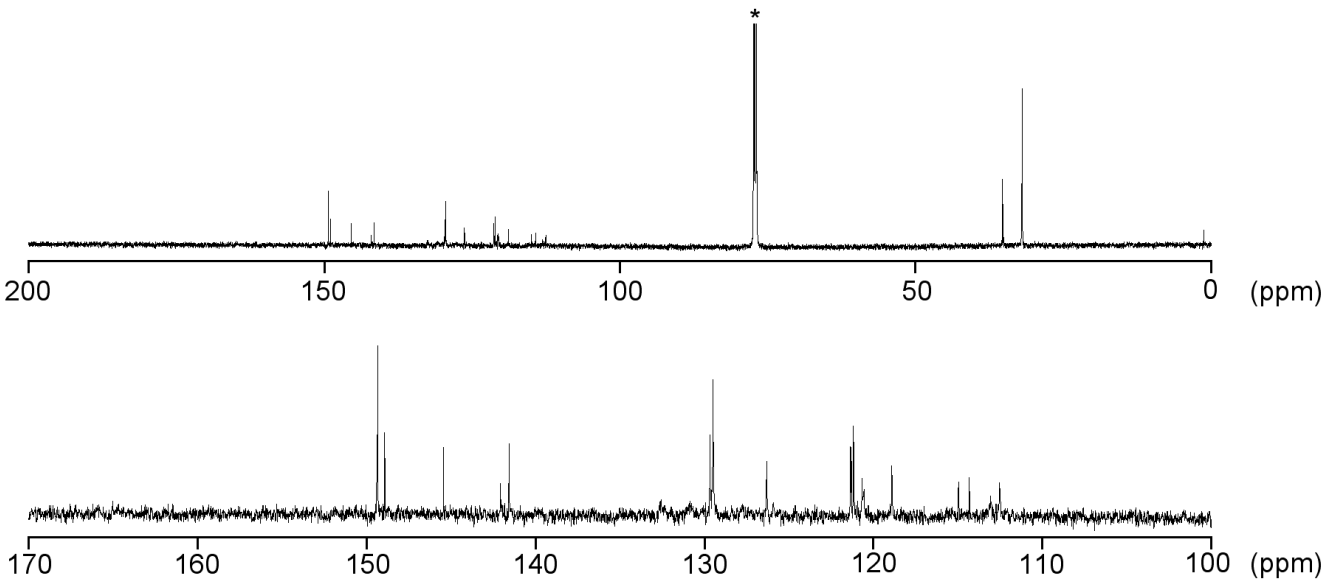

Figure S 10. ^{13}C NMR spectrum of **4H$_2$** in $CDCl_3$ at 25 °C. *Solvent.

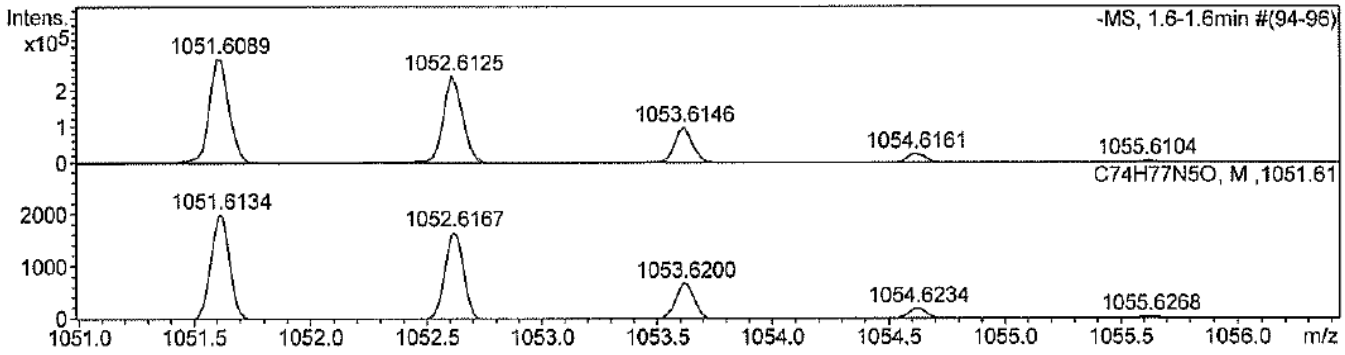

Figure S 11. Observed (top) and simulated (bottom) HR-APCI-TOF MS of **4H**$_2$.

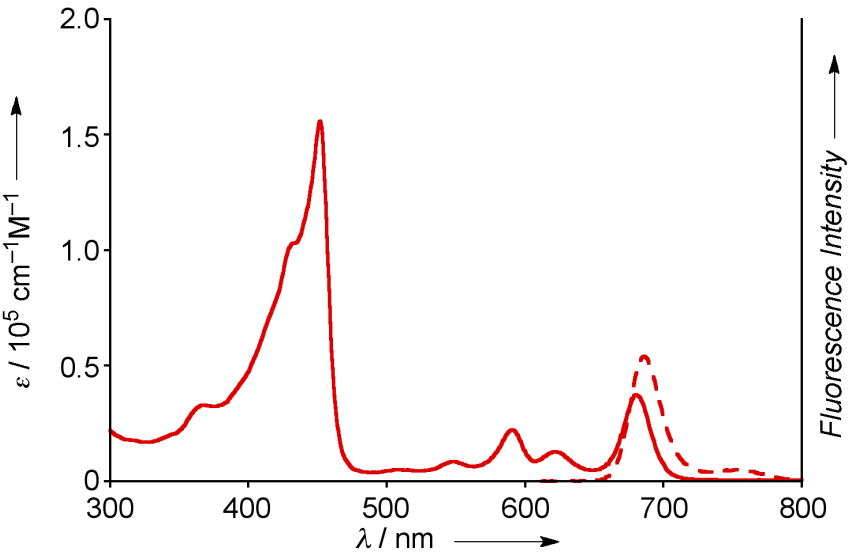

Figure S 12. UV/Vis absorption (solid line) and emission (dashed line) spectra of **4H**$_2$ in CH_2Cl_2.

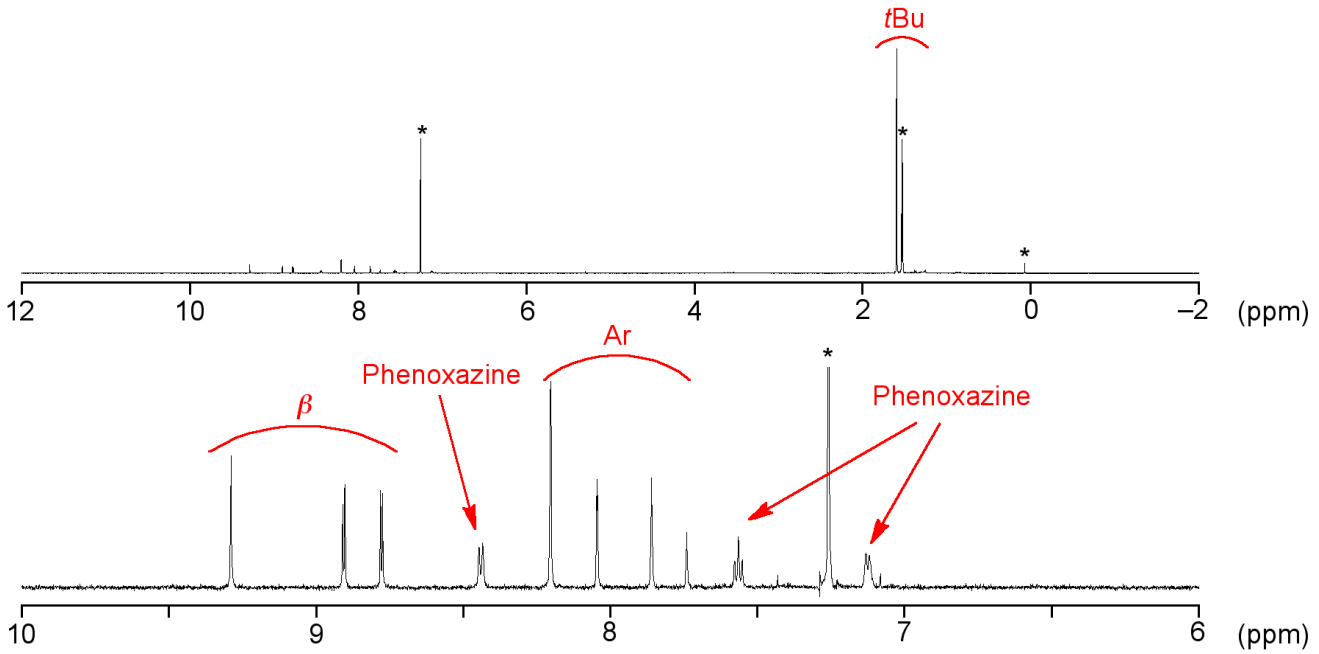

Figure S 13. ^{1}H NMR spectrum of **4Zn** in $CDCl_3$ at 25 °C. *Solvent.

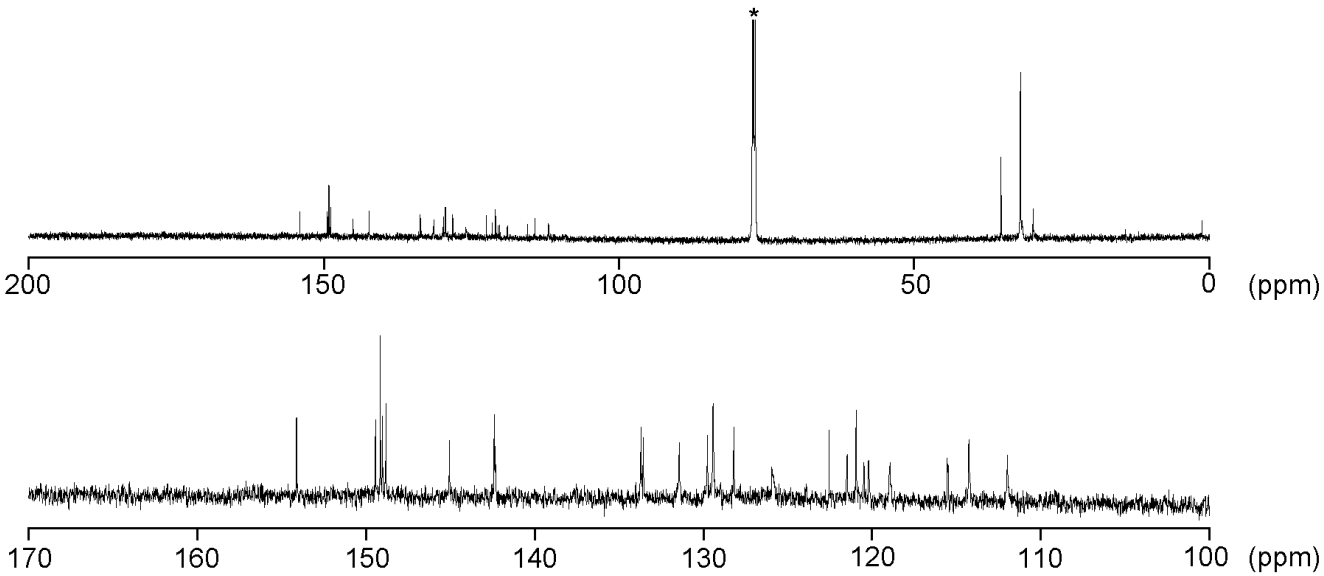

Figure S 14. ^{13}C NMR spectrum of **4Zn** in $CDCl_3$ at 25 °C. *Solvent.

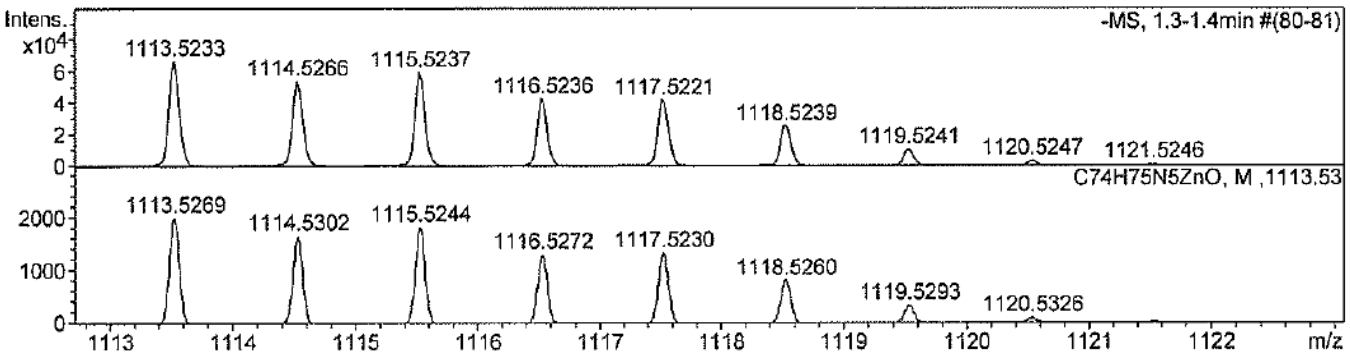

Figure S 15. Observed (top) and simulated (bottom) HR-APCI-TOF MS of **4Zn**.

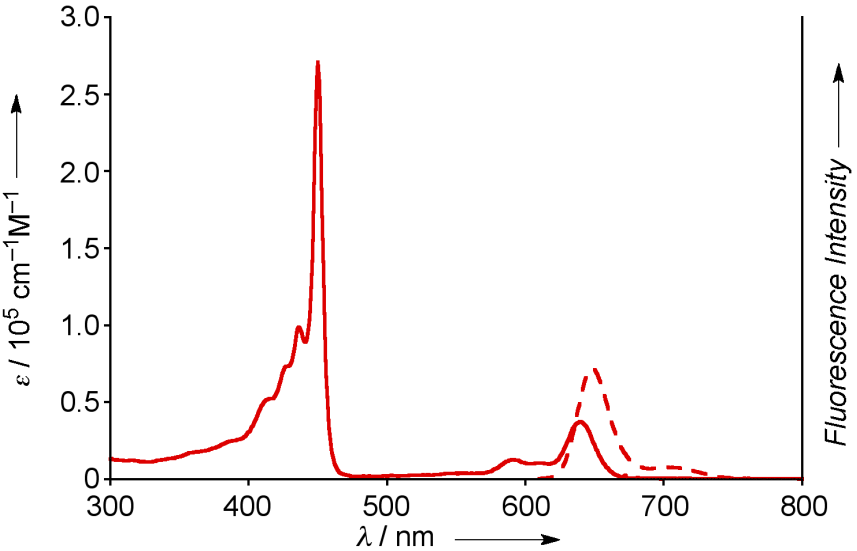

Figure S 16. UV/Vis absorption (solid line) and emission (dashed line) spectra of **4Zn** in CH_2Cl_2.

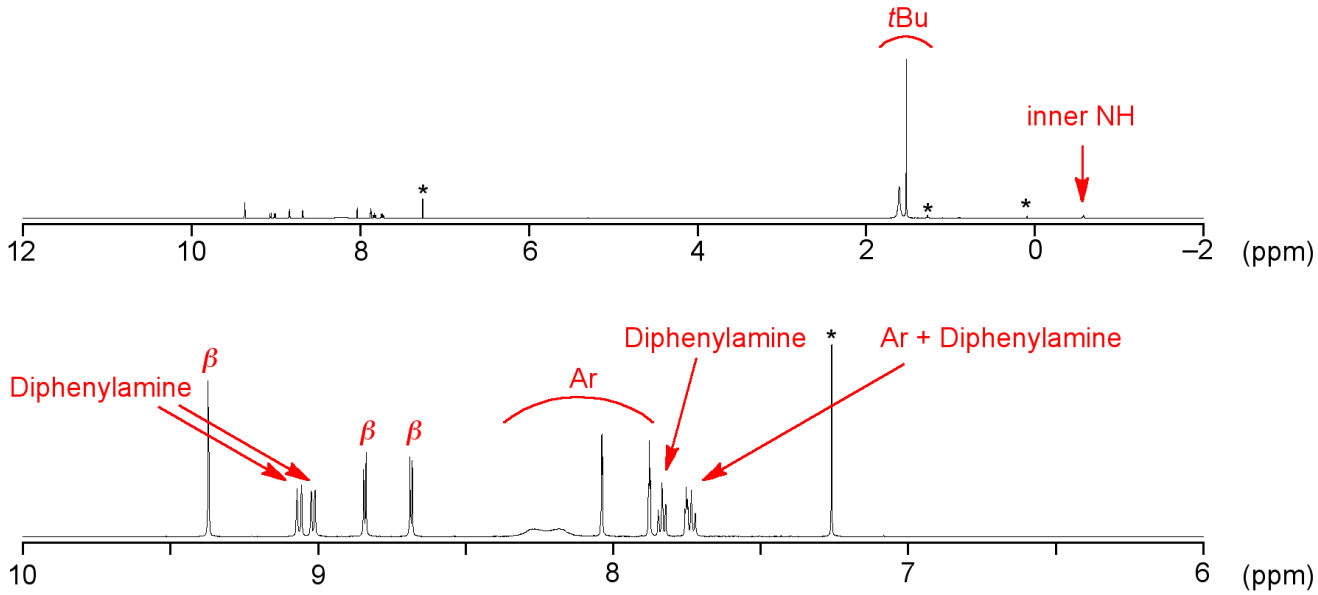

Figure S 17. ^{1}H NMR spectrum of **10H$_2$** in $CDCl_3$ at 25 °C. *Solvent and impurities.

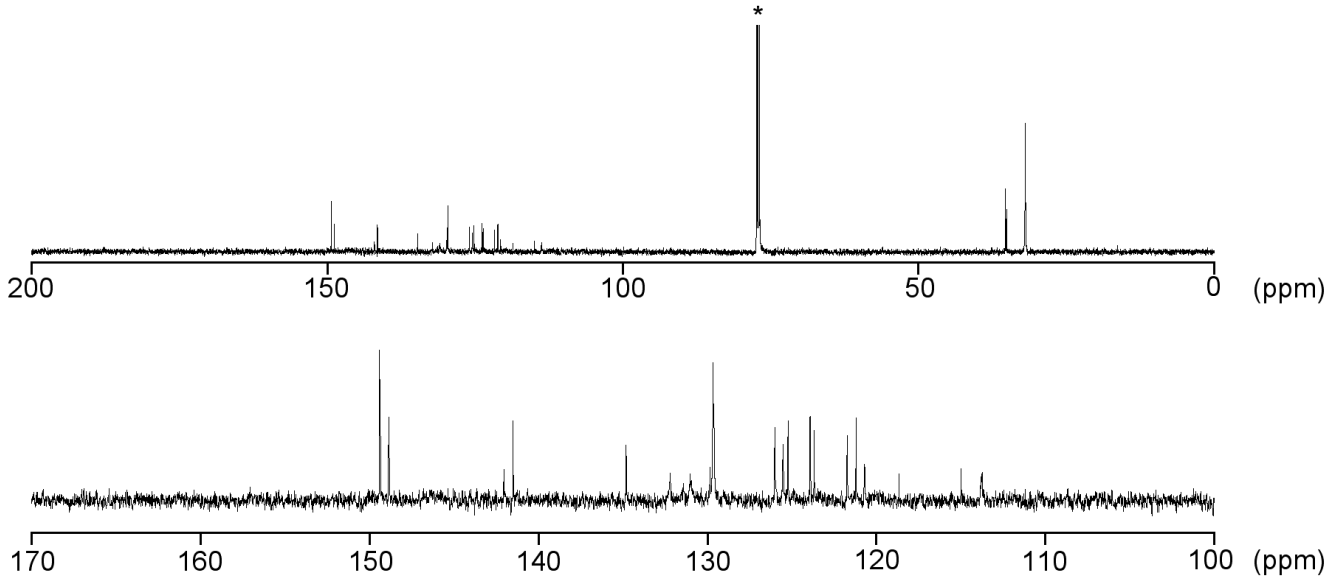

Figure S 18. ^{13}C NMR spectrum of **10H$_2$** in $CDCl_3$ at 25 °C. *Solvent.

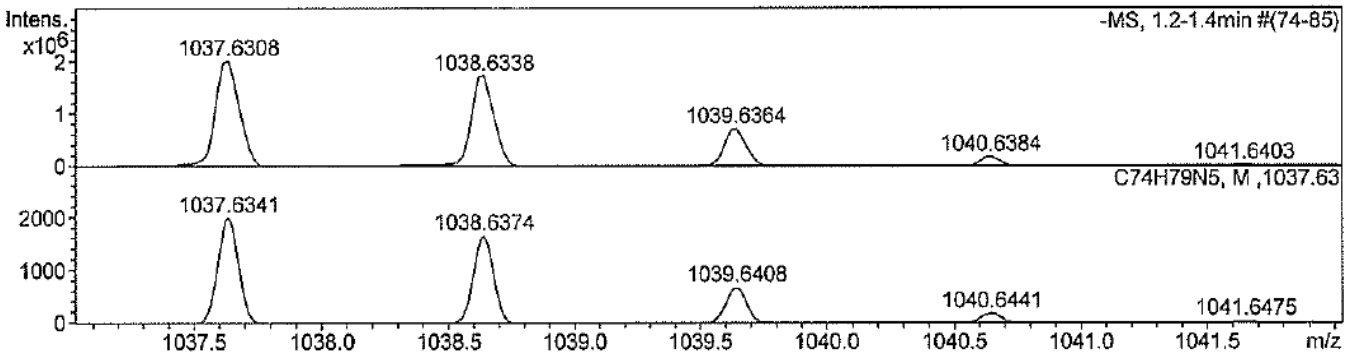

Figure S 19. Observed (top) and simulated (bottom) HR-APCI-TOF MS of **10H**$_2$.

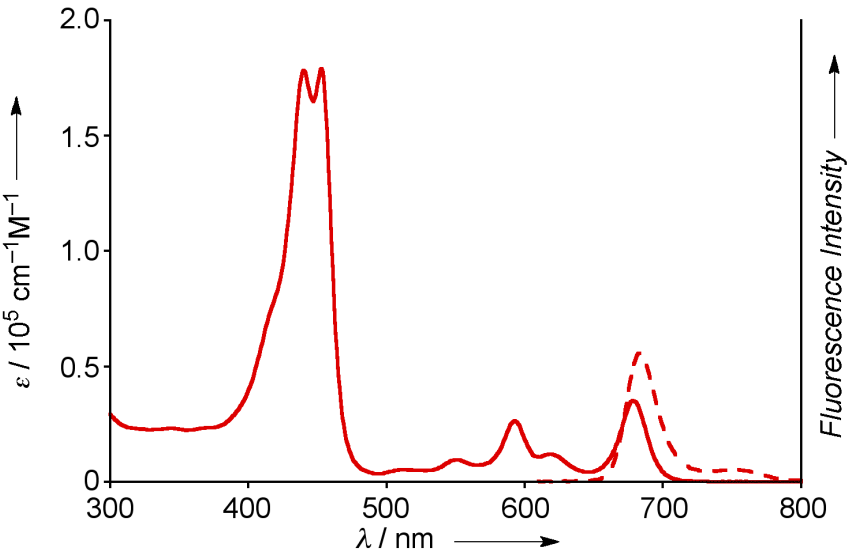

Figure S 20. UV/Vis absorption (solid line) and emission (dashed line) spectra of **10H**$_2$ in CH_2Cl_2.

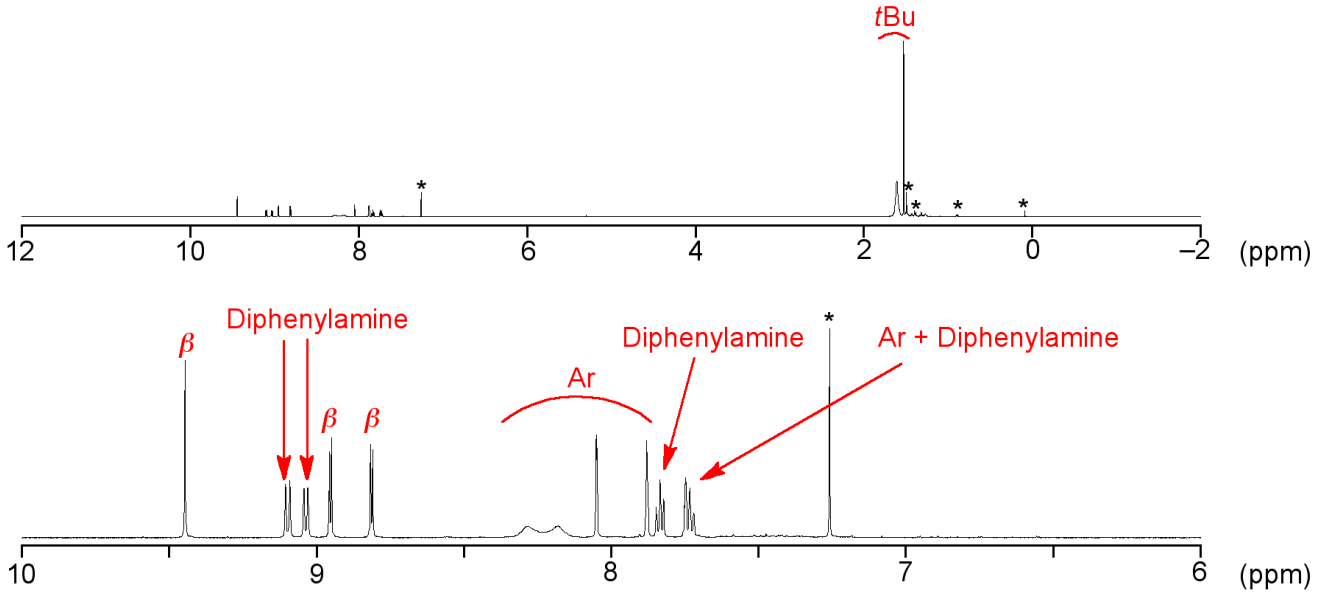

Figure S 21. ^{1}H NMR spectrum of **10Zn** in $CDCl_3$ at 25 °C. *Solvent and impurities.

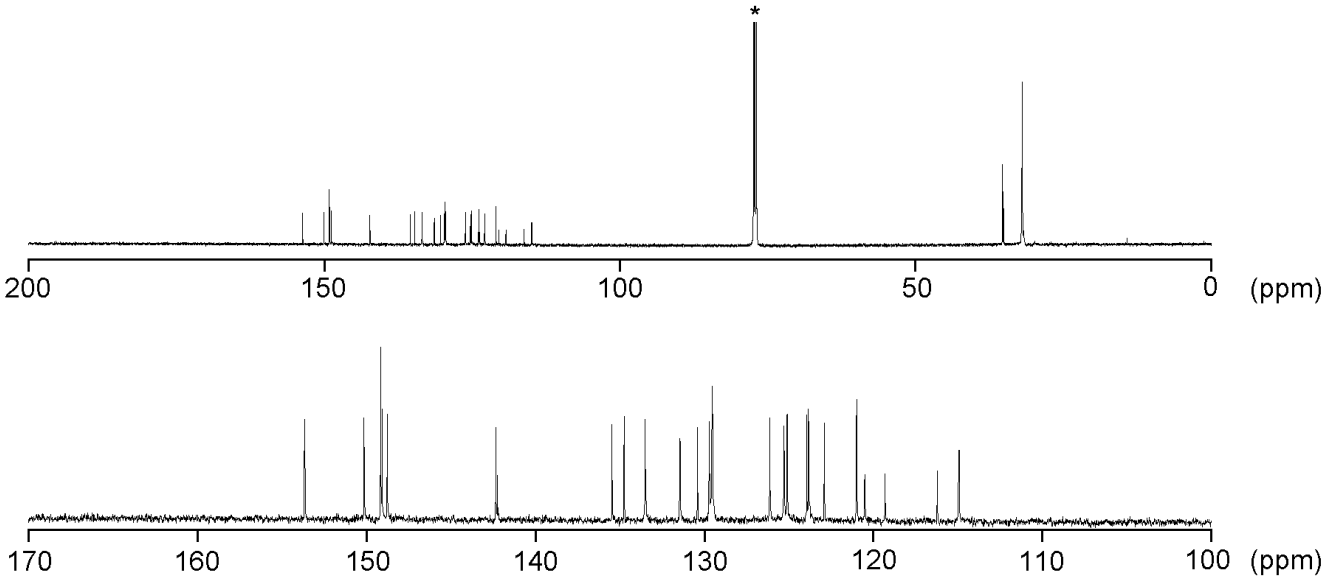

Figure S 22. ^{13}C NMR spectrum of **10Zn** in $CDCl_3$ at 25 °C. *Solvent.

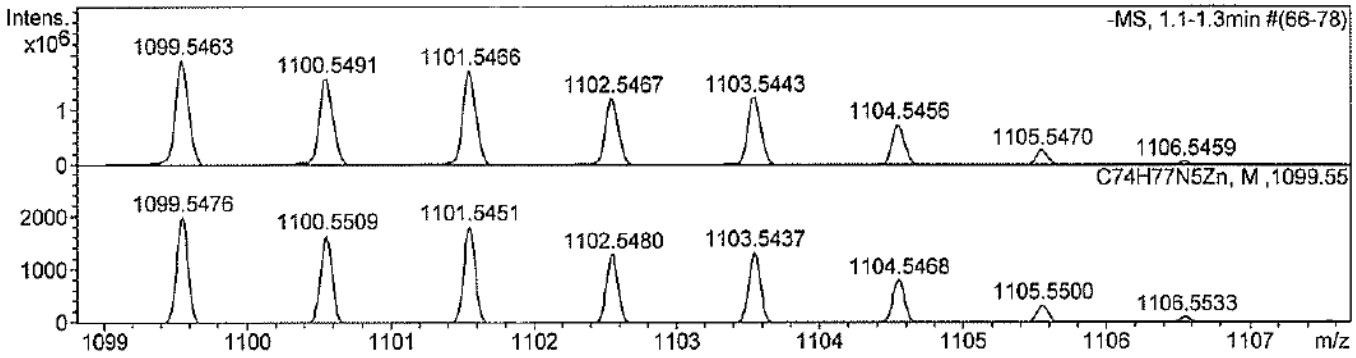

Figure S 23. Observed (top) and simulated (bottom) HR-APCI-TOF MS of **10Zn**.

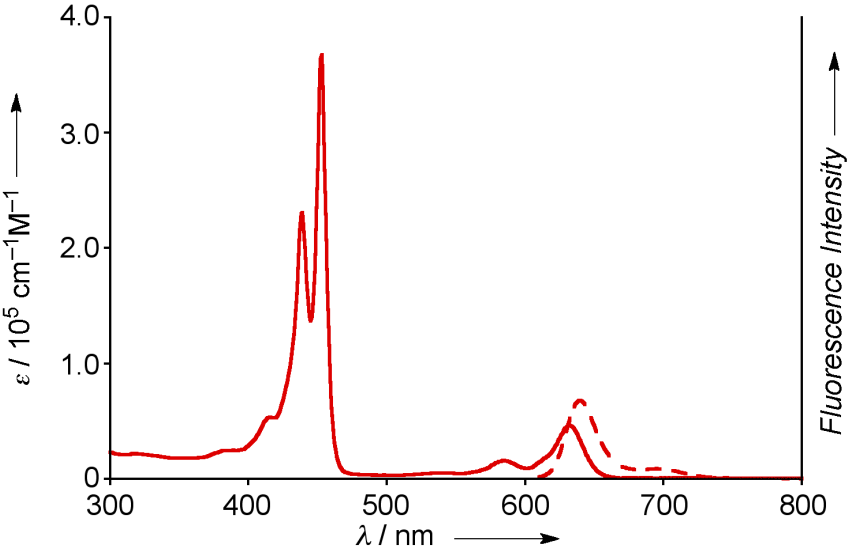

Figure S 24. UV/Vis absorption (solid line) and emission (dashed line) spectra of **10Zn** in CH_2Cl_2.

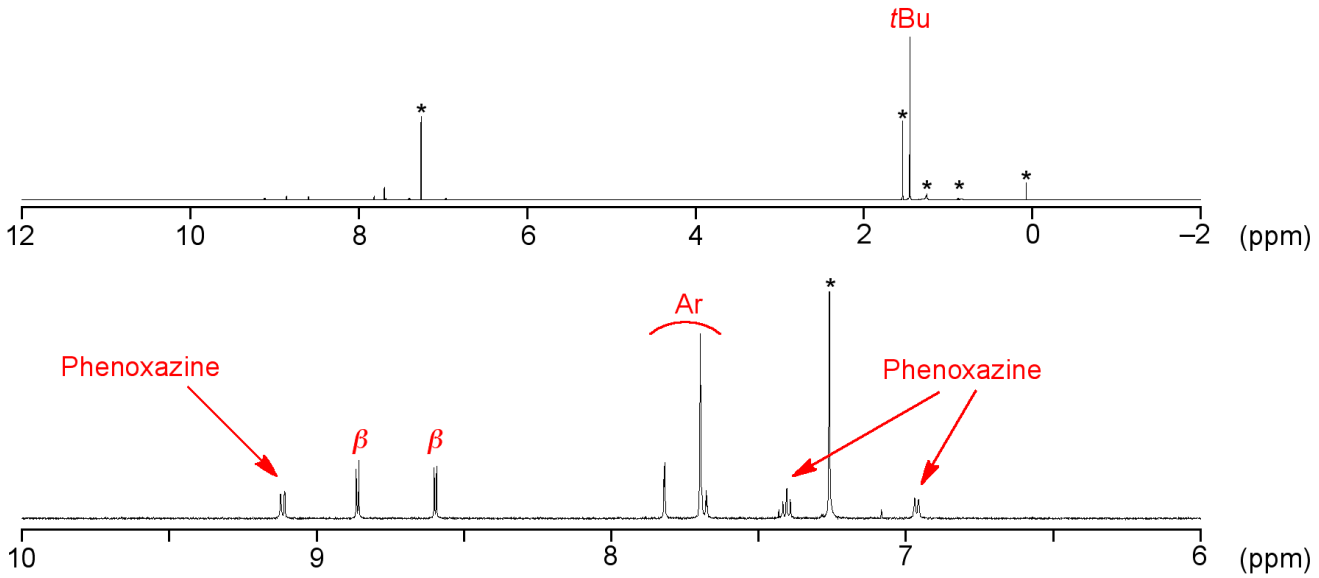

Figure S 25. ^{1}H NMR spectrum of **13** in $CDCl_3$ at 25 °C. *Solvent and impurities.

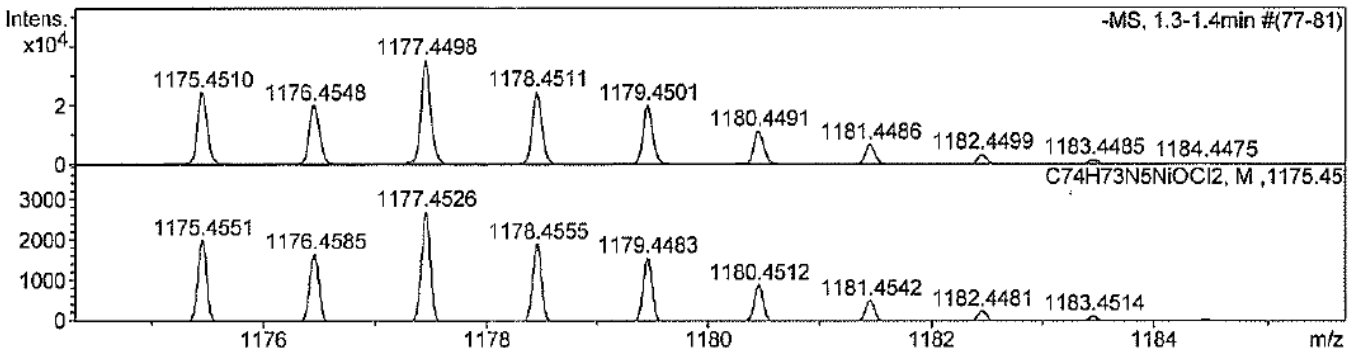

Figure S 26. Observed (top) and simulated (bottom) HR-APCI-TOF MS of **13**.

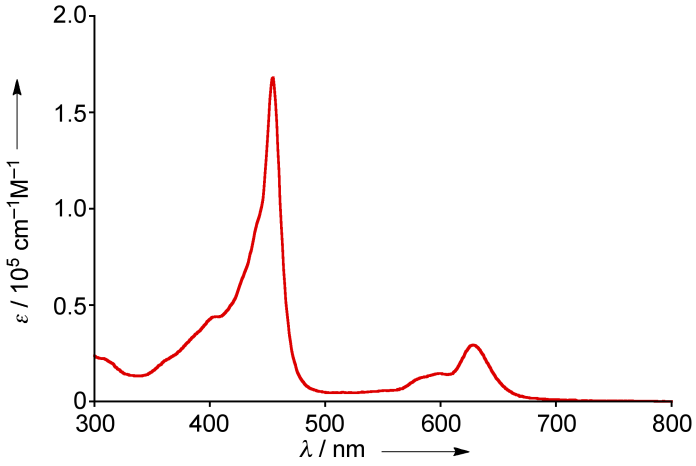

Figure S 27. UV/Vis absorption spectrum of **13** in CH_2Cl_2.

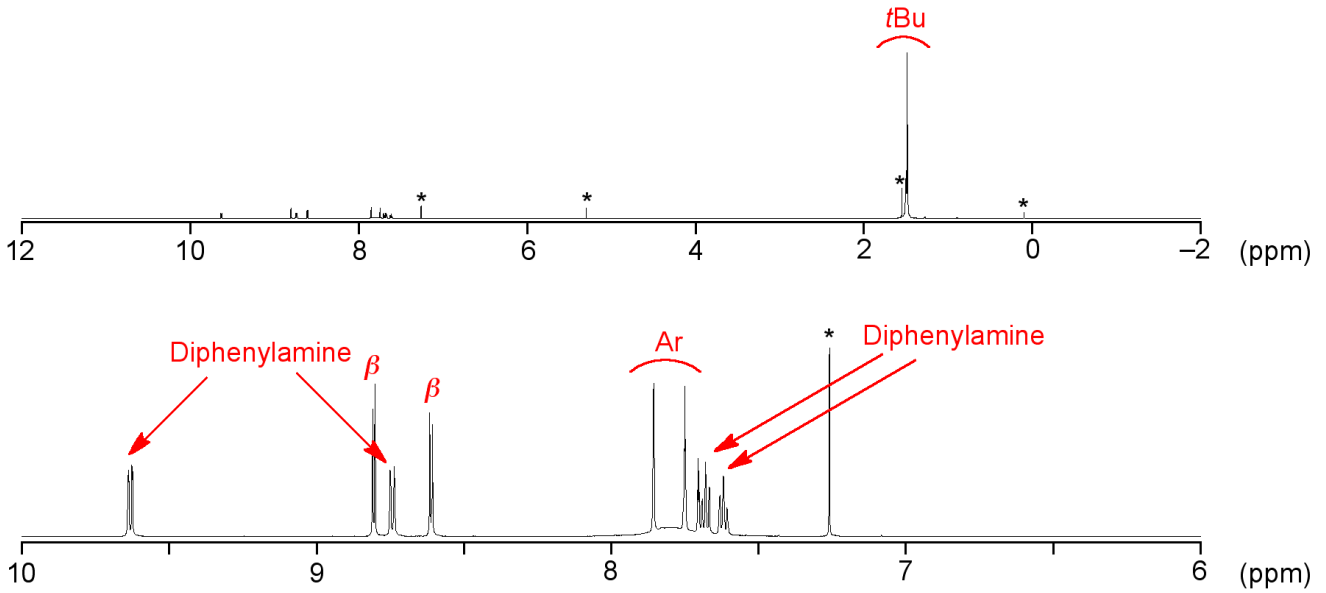

Figure S 28. ^{1}H NMR spectrum of **14** in $CDCl_3$ at 25 °C. *Solvent and impurities.

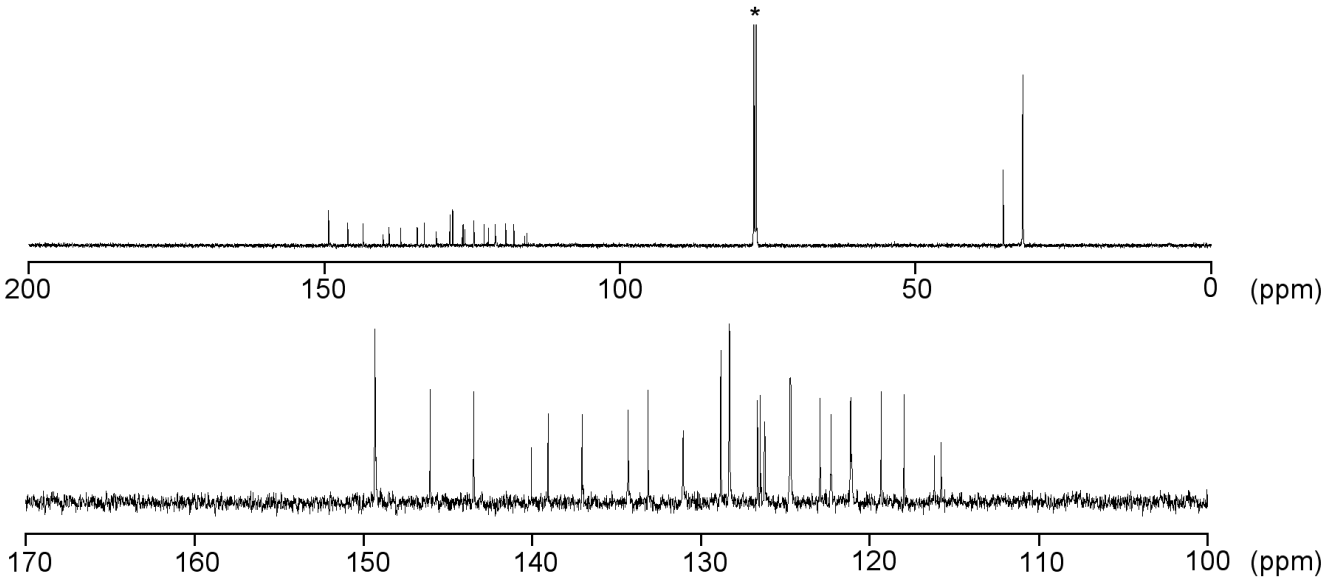

Figure S 29. ^{13}C NMR spectrum of **14** in $CDCl_3$ at 25 °C. *Solvent.

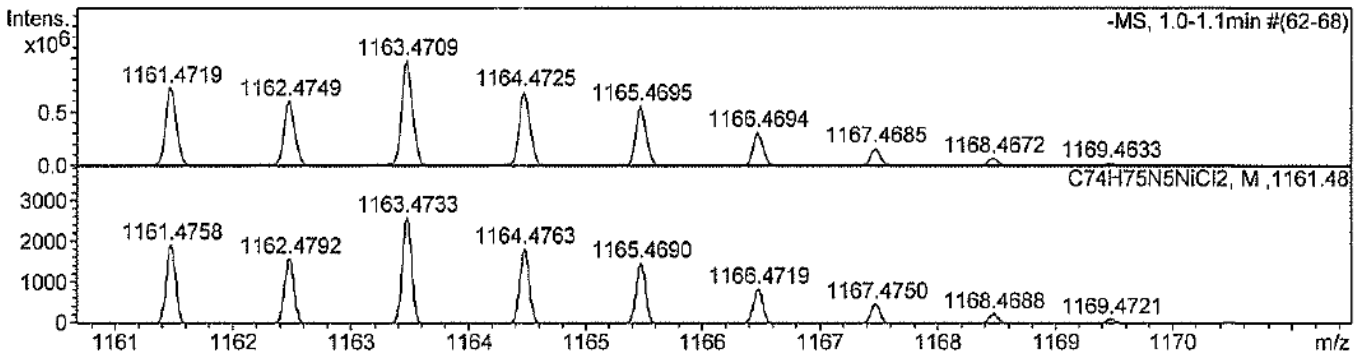

Figure S 30. Observed (top) and simulated (bottom) HR-APCI-TOF MS of **14**.

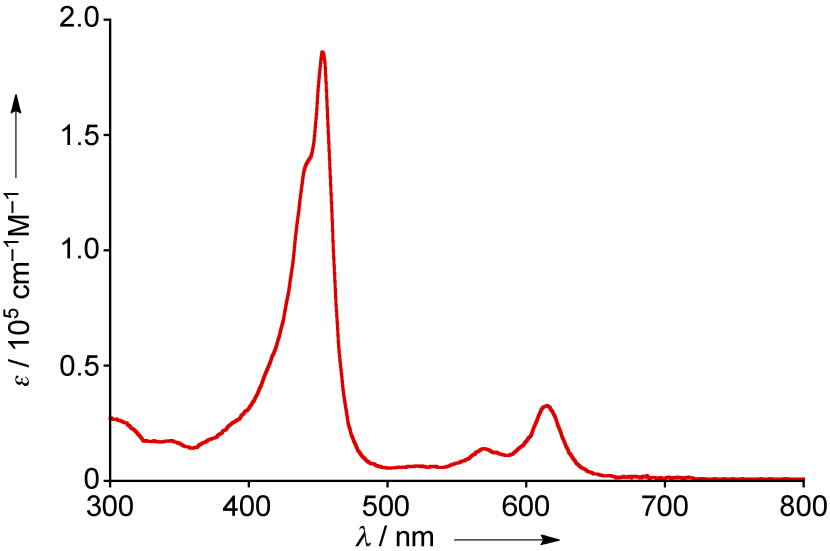

Figure S 31. UV/Vis absorption spectrum of **14** in CH_2Cl_2.

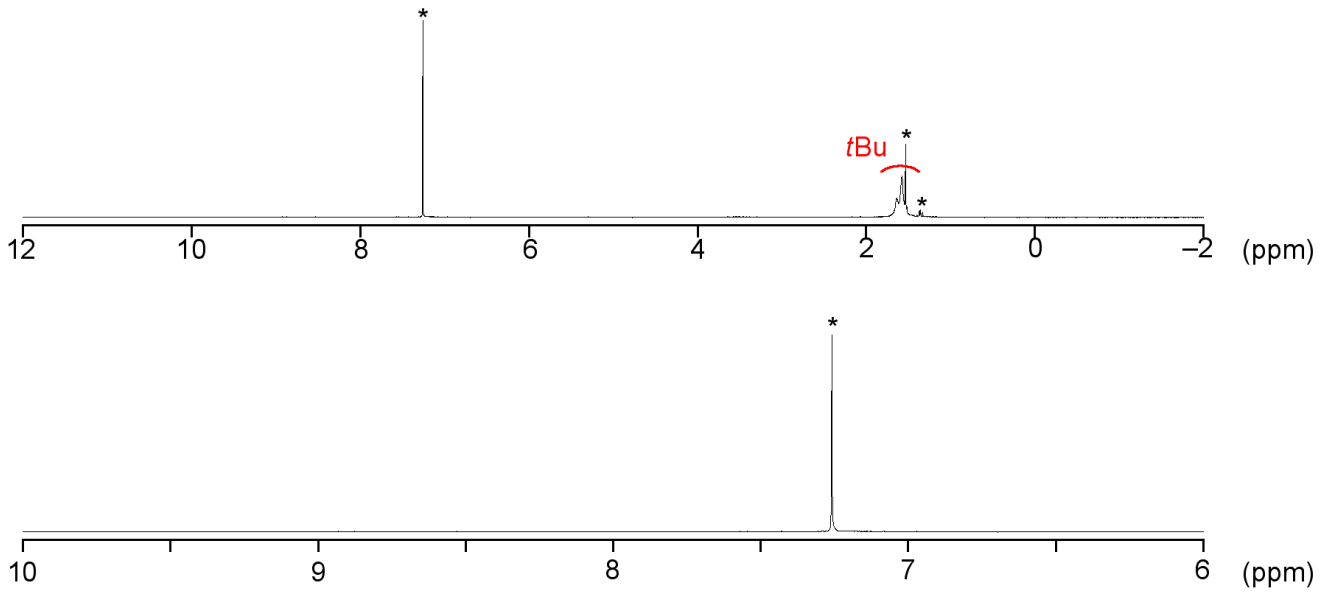

Figure S 32. ^{1}H NMR spectrum of **[13]**$^{+}$ in $CDCl_3$ at 25 °C. *Solvent and impurities.

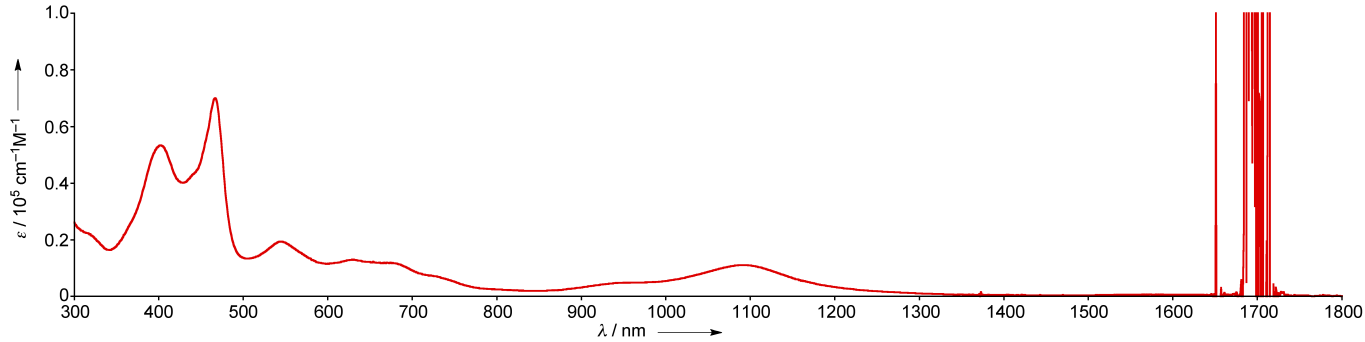

Figure S 33. UV/Vis absorption spectrum of **[13]**$^{+}$ in CH_2Cl_2.

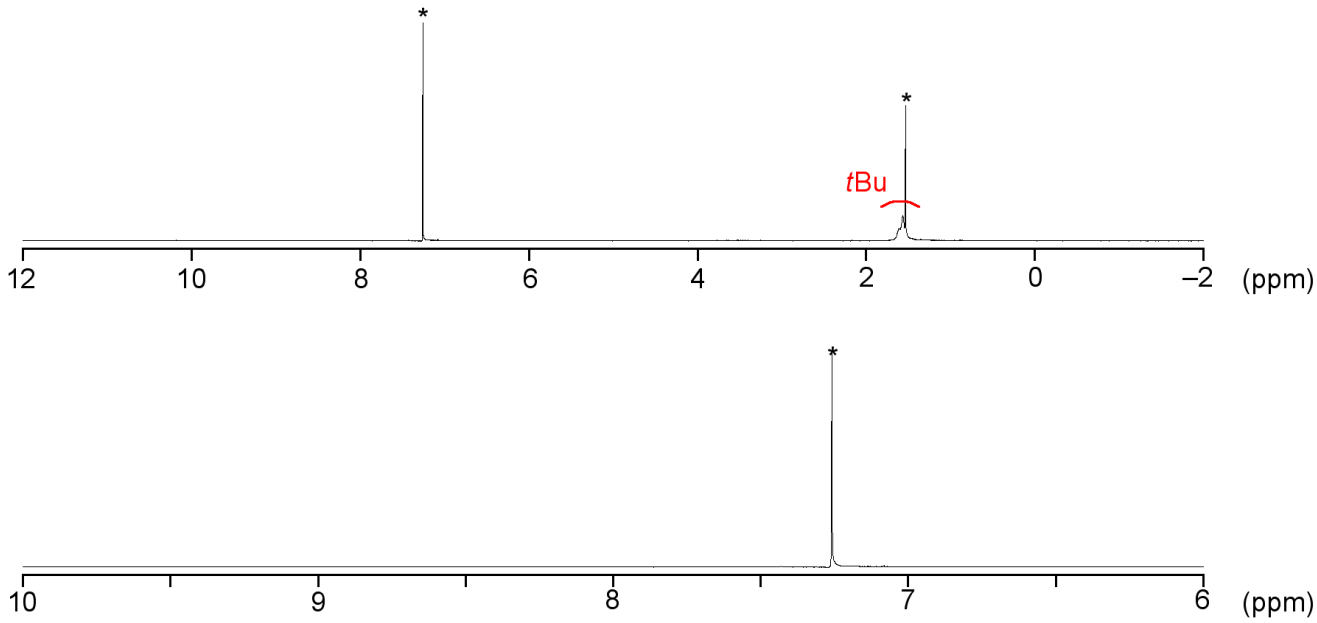

Figure S 34. ^{1}H NMR spectrum of **[14]**$^{+}$ in $CDCl_3$ at 25 °C. *Solvent and impurities.

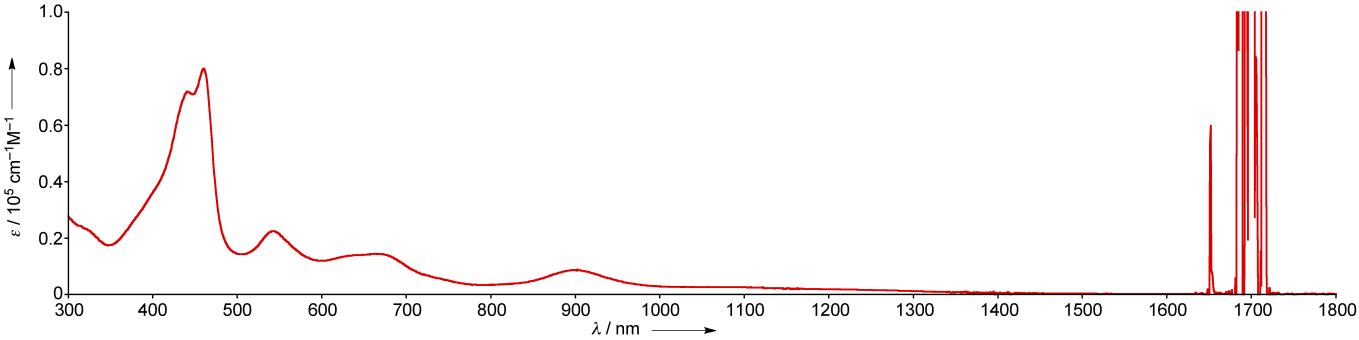

Figure S 35. UV/Vis absorption spectrum of **[14]**$^{+}$ in CH_2Cl_2.

4. ^{1}H NMR Dilution Titration[S2]

Estimation of the dimerisation constant (K_D)

$$2A \rightleftarrows A_2 \text{ for which } K_D = \frac{[A_2]}{[A]^2} \qquad (1)$$

Starting from the *law of mass action* expression for K_D in Eq. 1, we can write:

$$K_D = \frac{[A_2]}{(C - 2[A_2])^2} \qquad (2)$$

where $[A_2]$ is the dimer concentration and C is the total concentration of target compound in solution. Rearrangement of Eq. 2 gives:

$$\frac{1}{2}K_D C = \frac{2[A_2]}{C} + \frac{C}{2[A_2]} - 2 \qquad (3)$$

Then, replacing $\frac{2[A_2]}{C}$ by x gives Eq. 4.

$$\frac{1}{2}K_D C = x + \frac{1}{x} - 2 \qquad (4)$$

Therefore, the value of x, for which $0 < x < 1$, is given by:

$$x = \left(1 + \frac{K_D C}{4}\right) - \sqrt{\left(1 + \frac{K_D C}{4}\right)^2 - 1} \qquad (5)$$

The fraction x is related to the calculated chemical shift δ_{calc} through Eq. 6

$$x = \frac{(\delta_0 - \delta_{calc})}{(\delta_0 - \delta_\infty)} \qquad (6)$$

where δ_0 and δ_∞ are the chemical shifts of the free monomer and dimer, respectively. By using Eq. 5 and Eq. 6, δ_{calc} can be written as:

$$\delta_{calc} = \delta_0 + (\delta_\infty - \delta_0)\left(1 + \frac{1 - \sqrt{8K_D C + 1}}{4K^D C}\right) \qquad (6)$$

K_D value was estimated by minimizing the RSS-value (Eq. 7), by interatively varying K_D, δ_0, and δ_∞, using Solver in Microsoft Excel.

$$RSS = \sum(\delta_{obs} - \delta_{calc})^2 \qquad (7)$$

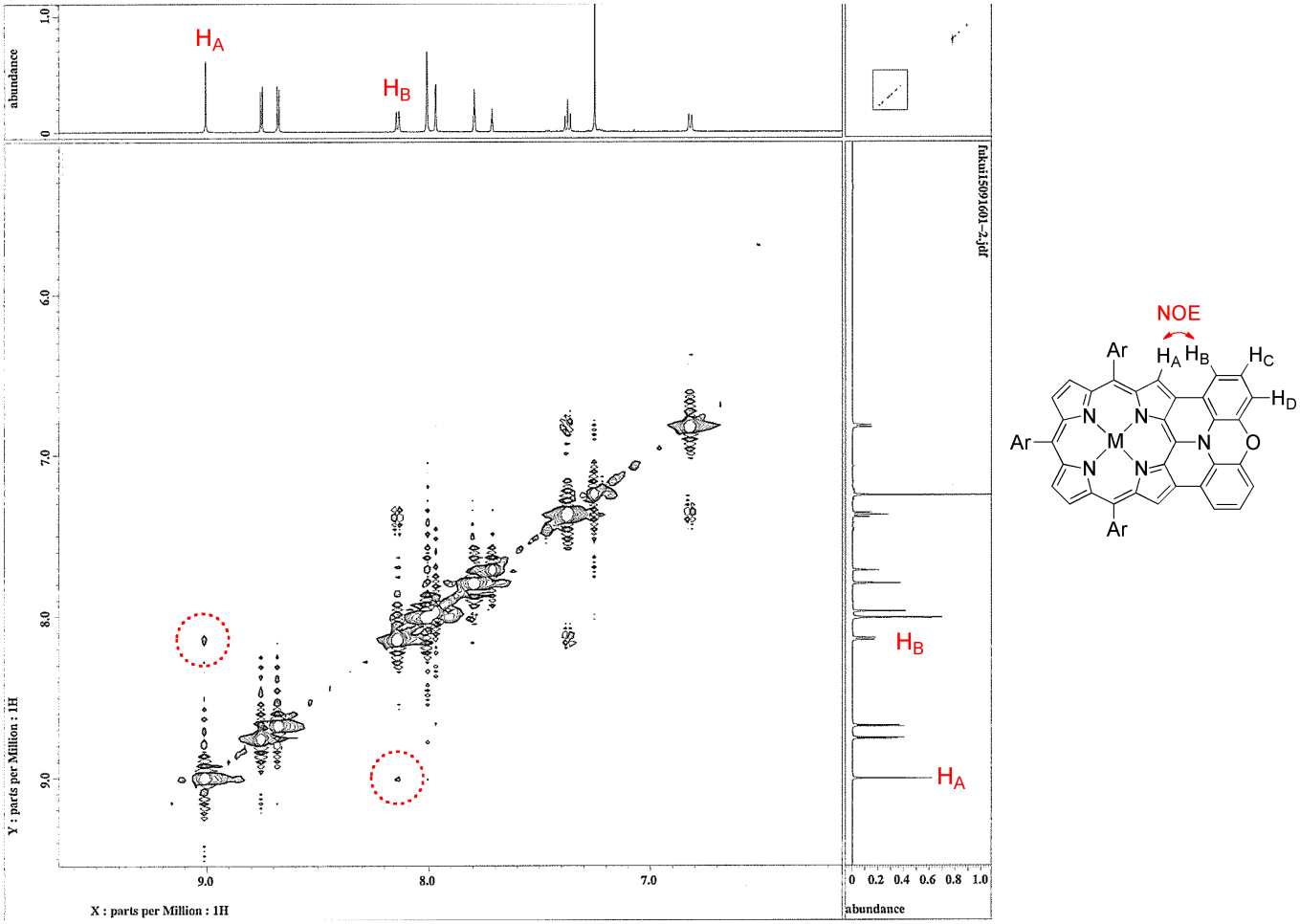

Figure S 36. NOESY spectrum of **4Ni** in $CDCl_3$ at 25 °C.

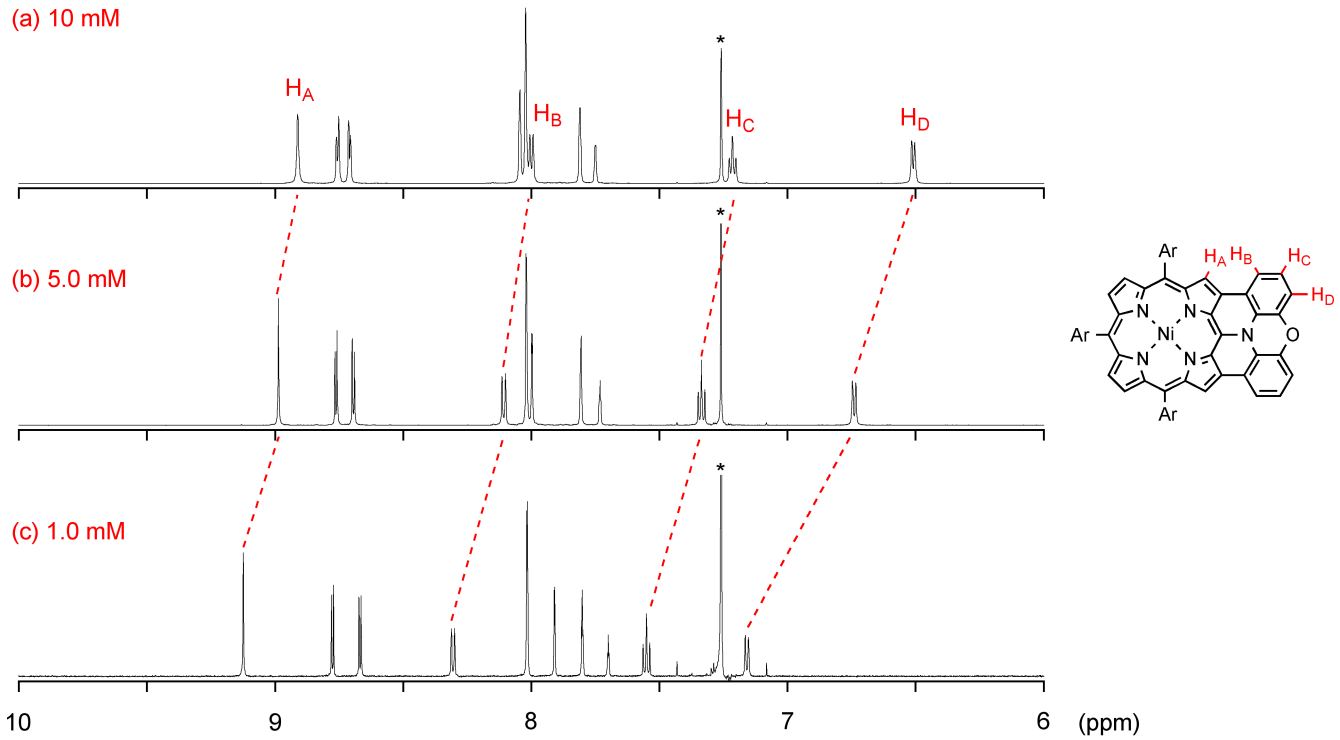

Figure S 37. ^{1}H NMR spectra of **4Ni** in $CDCl_3$ under different concentrations: (a) 10 mM, (b) 5.0 mM, and (c) 1.0 mM at 25 °C.

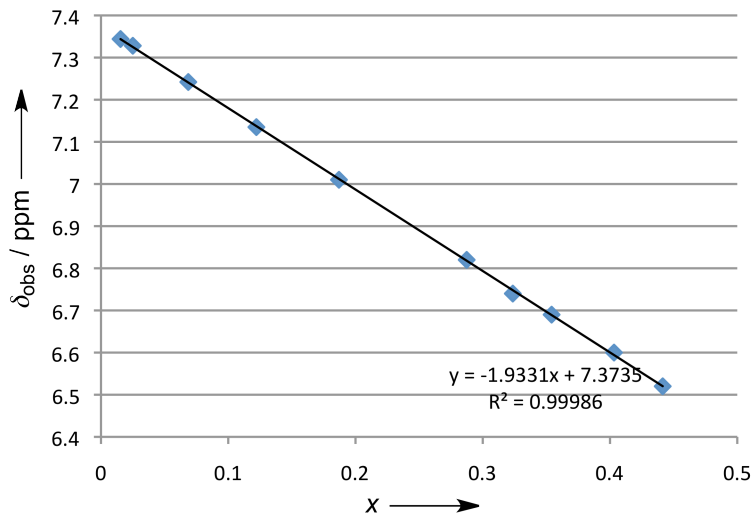

C (mM)	*x*	δ_{obs} of H_D (ppm)
10.0	0.441	6.52
8.0	0.403	6.60
6.0	0.354	6.69
5.0	0.324	6.74
4.0	0.287	6.82
2.0	0.187	7.01
1.1	0.122	7.14
0.56	0.069	7.24
0.19	0.025	7.33
0.11	0.015	7.34

$K_D = 7.2 \times 10\ M^{-1}$

Figure S 38. ^{1}H NMR dilution titration of **4Ni**.

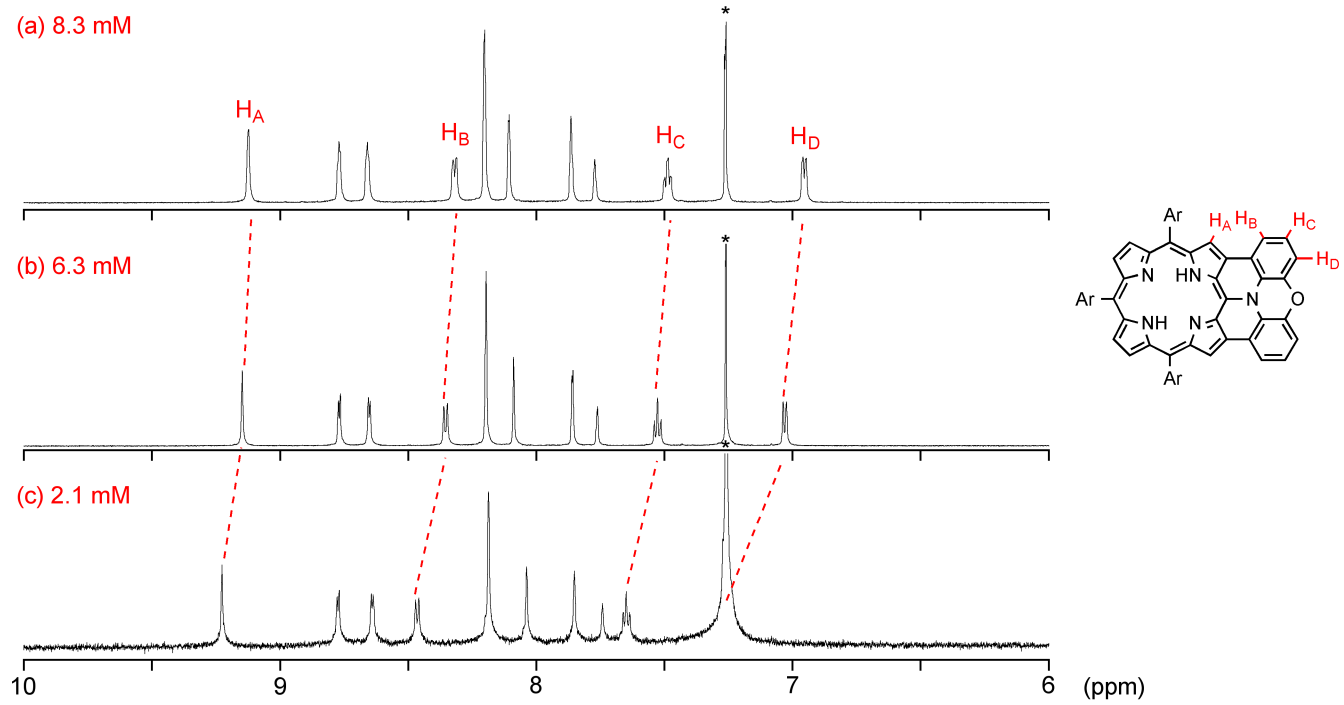

Figure S 39. ^{1}H NMR spectra of **4H$_2$** in $CDCl_3$ under different concentrations: (a) 8.3 mM, (b) 6.3 mM, and (c) 2.1 mM at 25 °C.

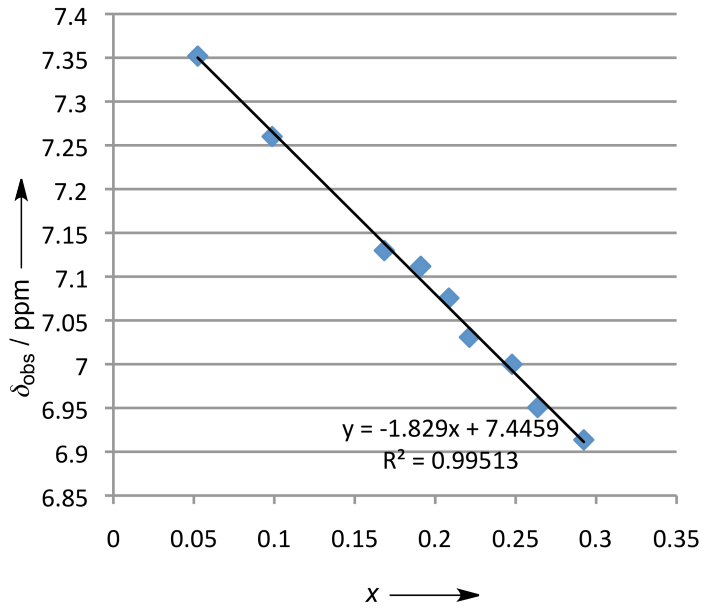

C (mM)	*x*	δ_{obs} of H_D (ppm)
10.0	0.292	6.91
8.3	0.264	6.95
7.5	0.245	7.00
6.3	0.221	7.03
5.7	0.208	7.08
5.0	0.191	7.11
4.2	0.168	7.13
2.1	0.099	7.26
1.0	0.052	7.35

$K_D = 2.9 \times 10\ M^{-1}$

Figure S 40. ^{1}H NMR dilution titration of **4H$_2$**.

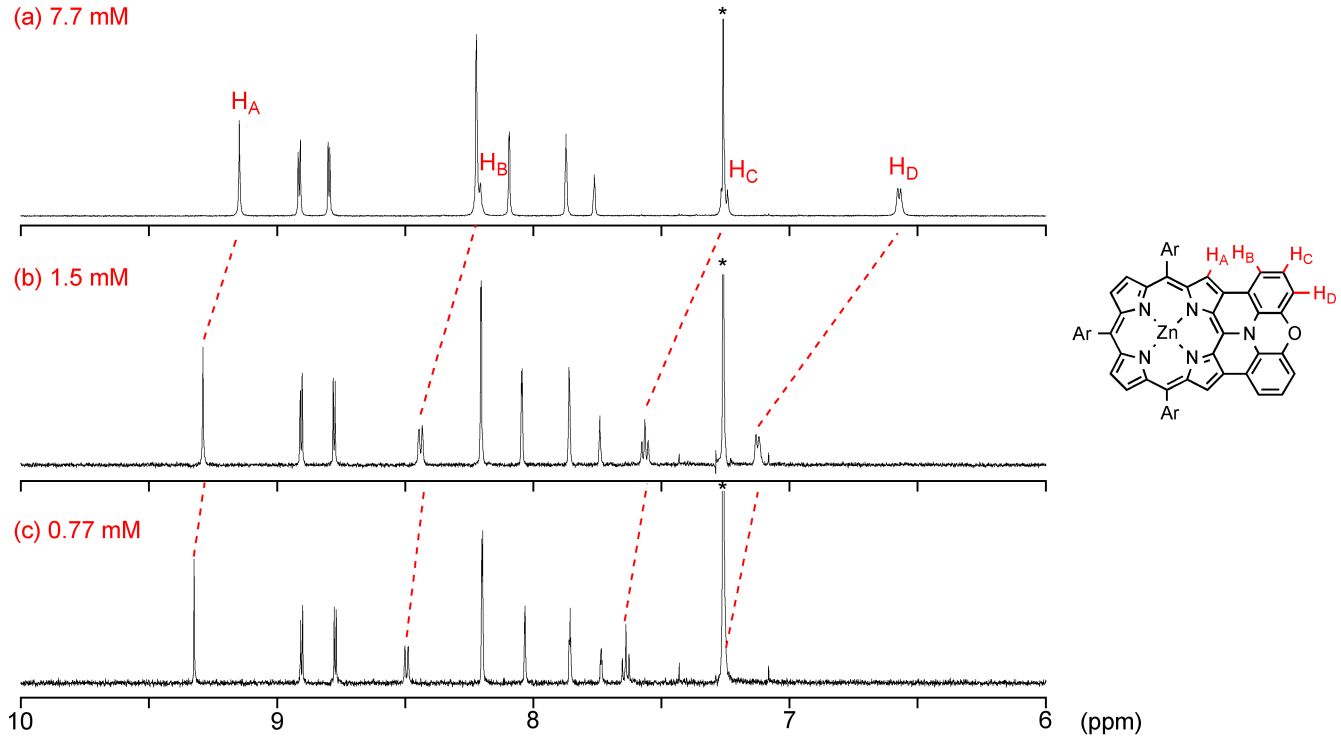

Figure S 41. ^{1}H NMR spectra of **4Zn** in $CDCl_3$ under different concentrations: (a) 8.3 mM, (b) 6.3 mM, and (c) 2.1 mM at 25 °C.

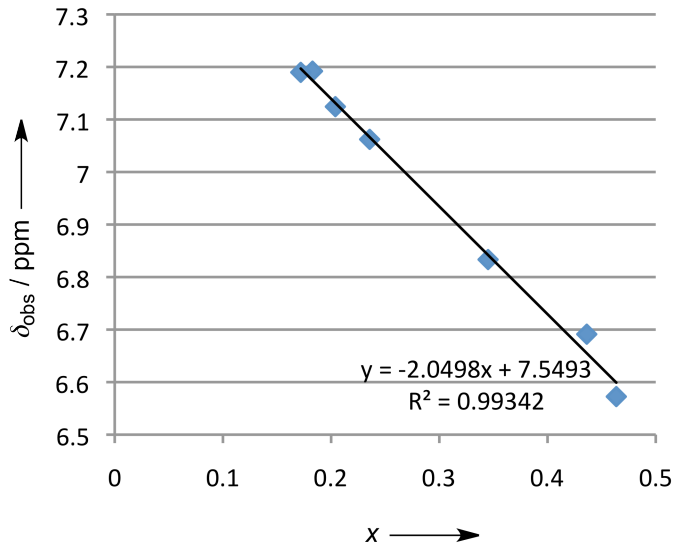

C (mM)	*x*	δ_{obs} of H_D (ppm)
7.7	0.464	6.57
6.6	0.436	7.19
3.9	0.345	6.83
1.9	0.236	7.06
1.5	0.204	7.12
1.3	0.183	7.19
0.77	0.464	6.57

$K_D = 1.0 \times 10^2\ M^{-1}$

Figure S 42. ^{1}H NMR dilution titration of **4Zn**.

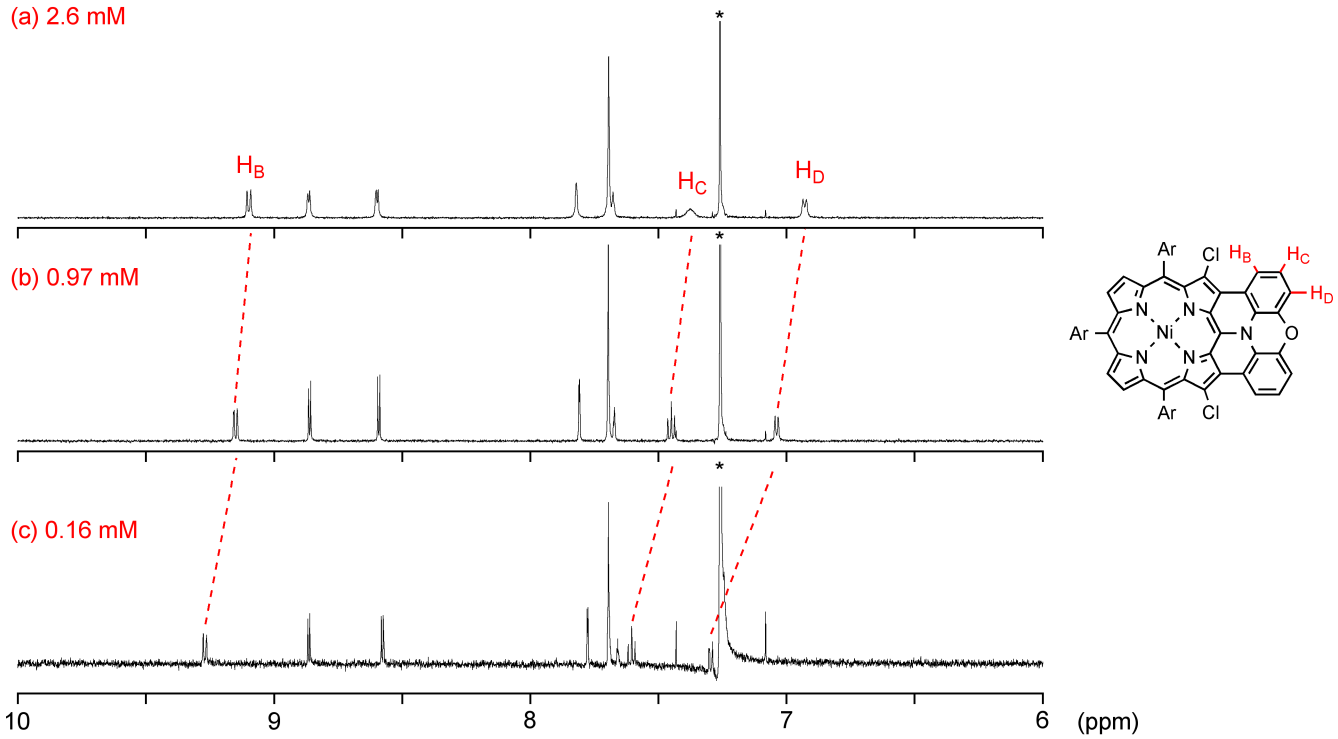

Figure S 43. ^{1}H NMR spectra of **13** in $CDCl_3$ under different concentrations: (a) 2.6 mM, (b) 0.97 mM, and (c) 0.16 mM at 25 °C.

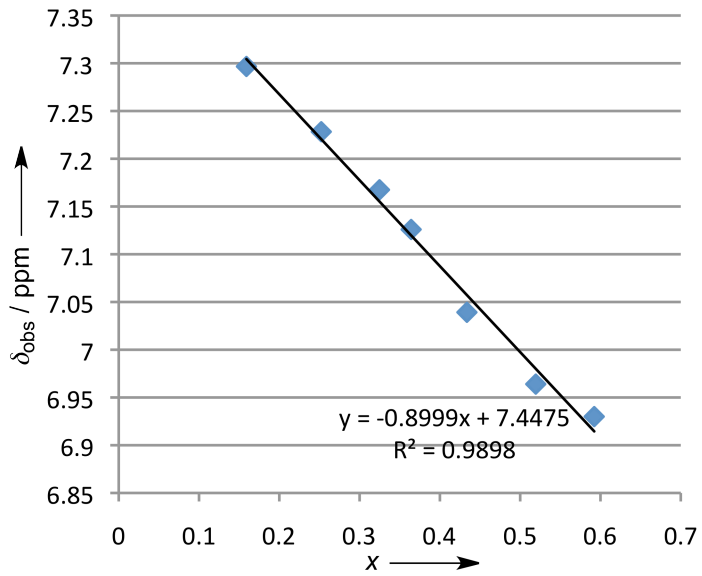

C (mM)	*x*	δ_{obs} of H_D (ppm)
2.6	0.592	6.93
1.6	0.519	6.96
0.97	0.434	7.04
0.65	0.364	7.13
0.51	0.325	7.17
0.32	0.252	7.23
0.16	0.159	7.30

$K_D = 7.0 \times 10^2\ M^{-1}$

Figure S 44. ^{1}H NMR dilution titration of **13**.

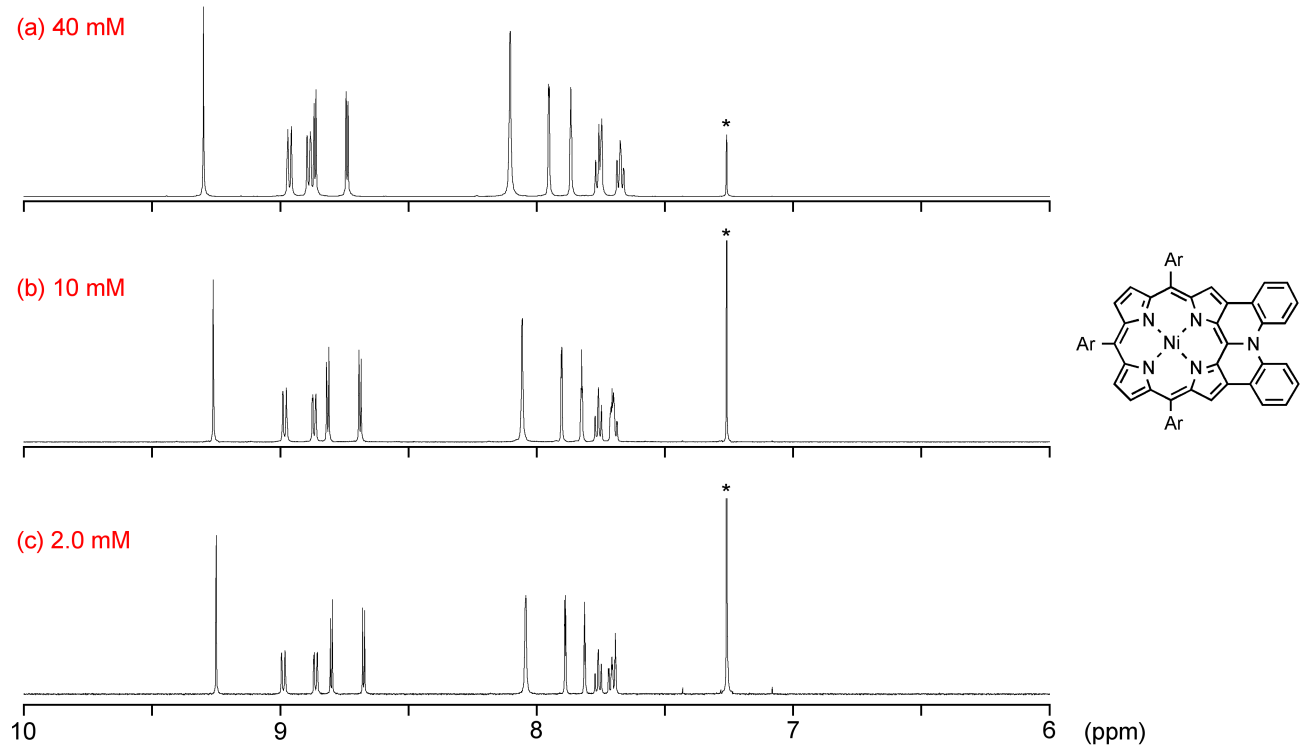

Figure S 45. ^{1}H NMR spectra of **10Ni** in $CDCl_3$ under different concentrations: (a) 40 mM, (b) 10 mM, and (c) 2.0 mM at 25 °C.

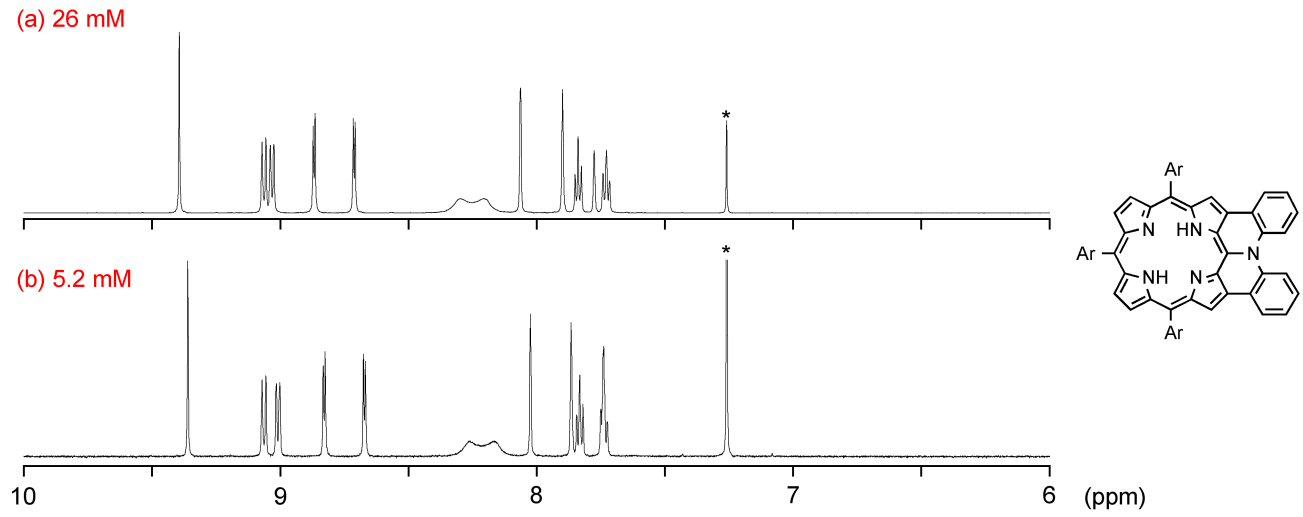

Figure S 46. ^{1}H NMR spectra of **10H$_2$** in $CDCl_3$ under different concentrations: (a) 26 mM and (c) 5.2 mM at 25 °C.

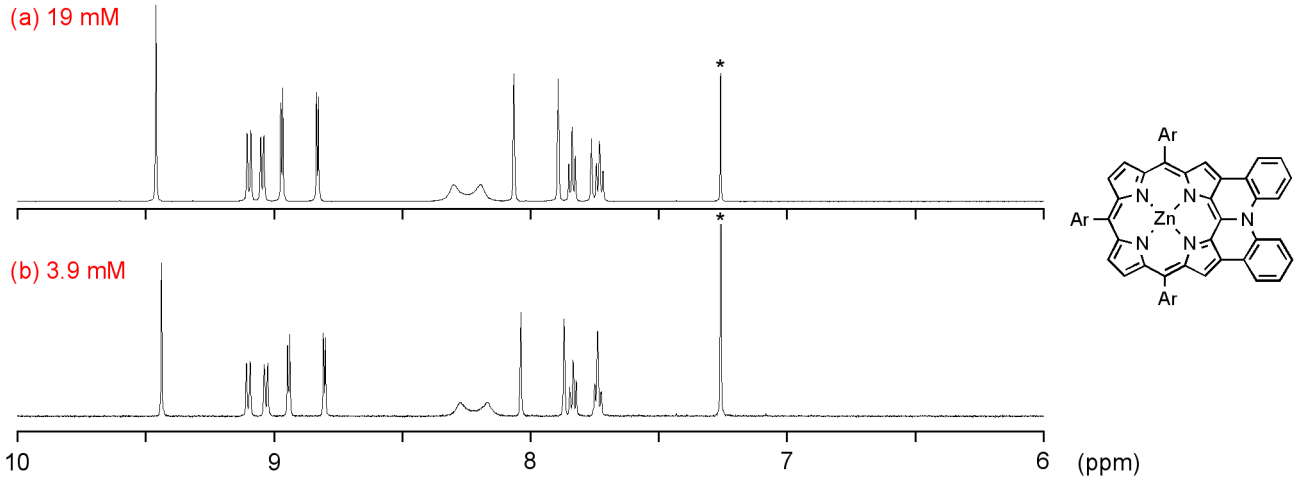

Figure S 47. ^{1}H NMR spectra of **10Zn** in $CDCl_3$ under different concentrations: (a) 19 mM and (c) 3.9 mM at 25 °C.

5. X-Ray Crystal Structures

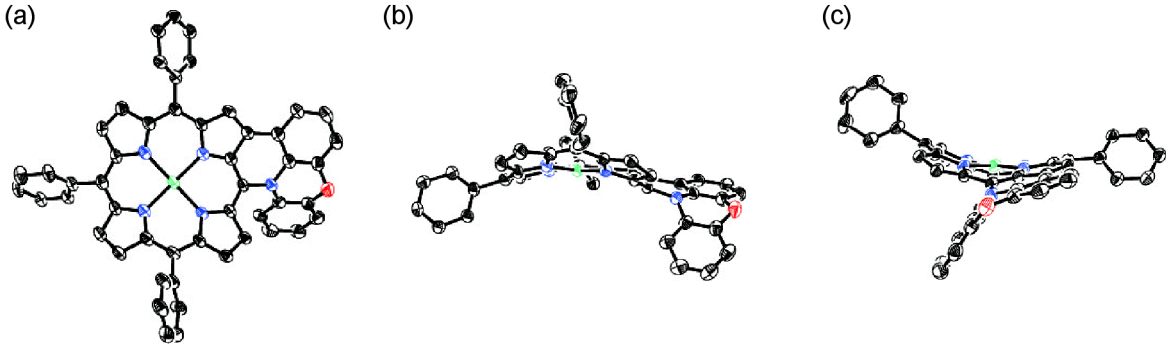

Figure S 48. X-Ray crystal structures of **9**. (a) Top view and (b,c) side views. Thermal ellipsoids are shown at the 50% probability level. Solvent molecules, *tert*-butyl groups, and all hydrogen atoms are omitted for clarity.

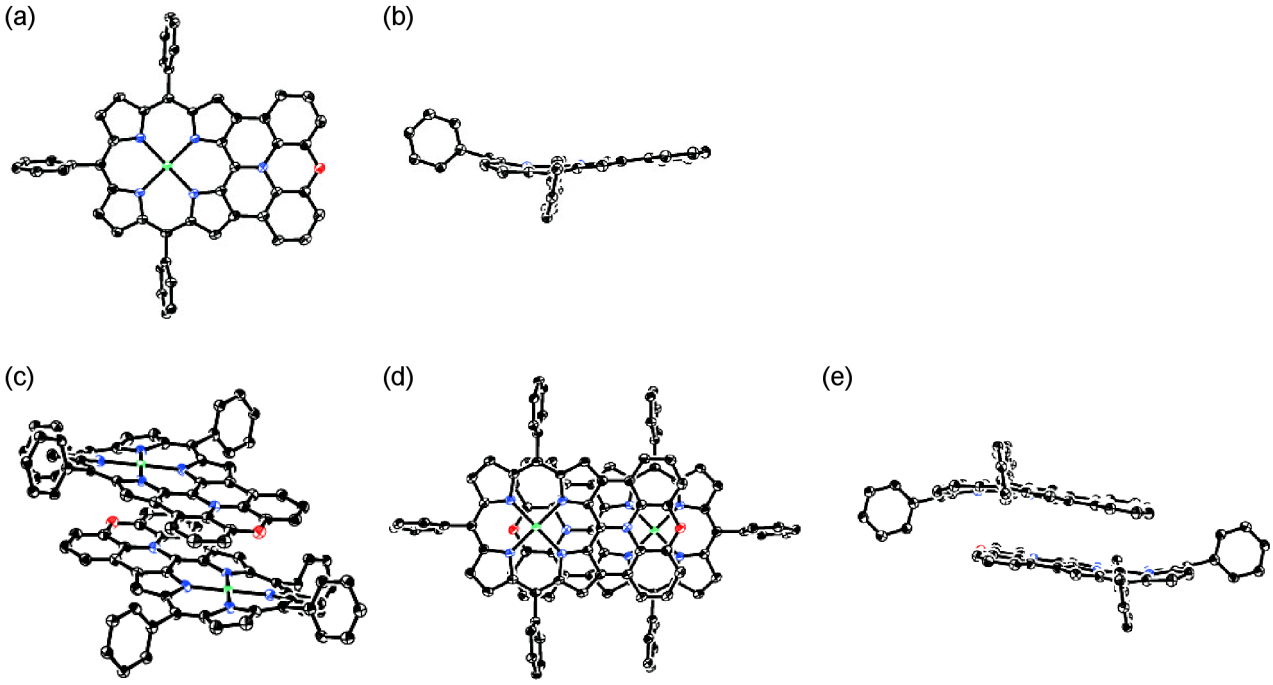

Figure S 49. X-Ray crystal structures of **4Ni**. (a) Top view and (b) side view of the single molecule. (c) Over view, (d) top view, and (e) side view of the π-stacked dimer. Thermal ellipsoids are shown at the 50% probability level. Solvent molecules, *tert*-butyl groups, and all hydrogen atoms are omitted for clarity.

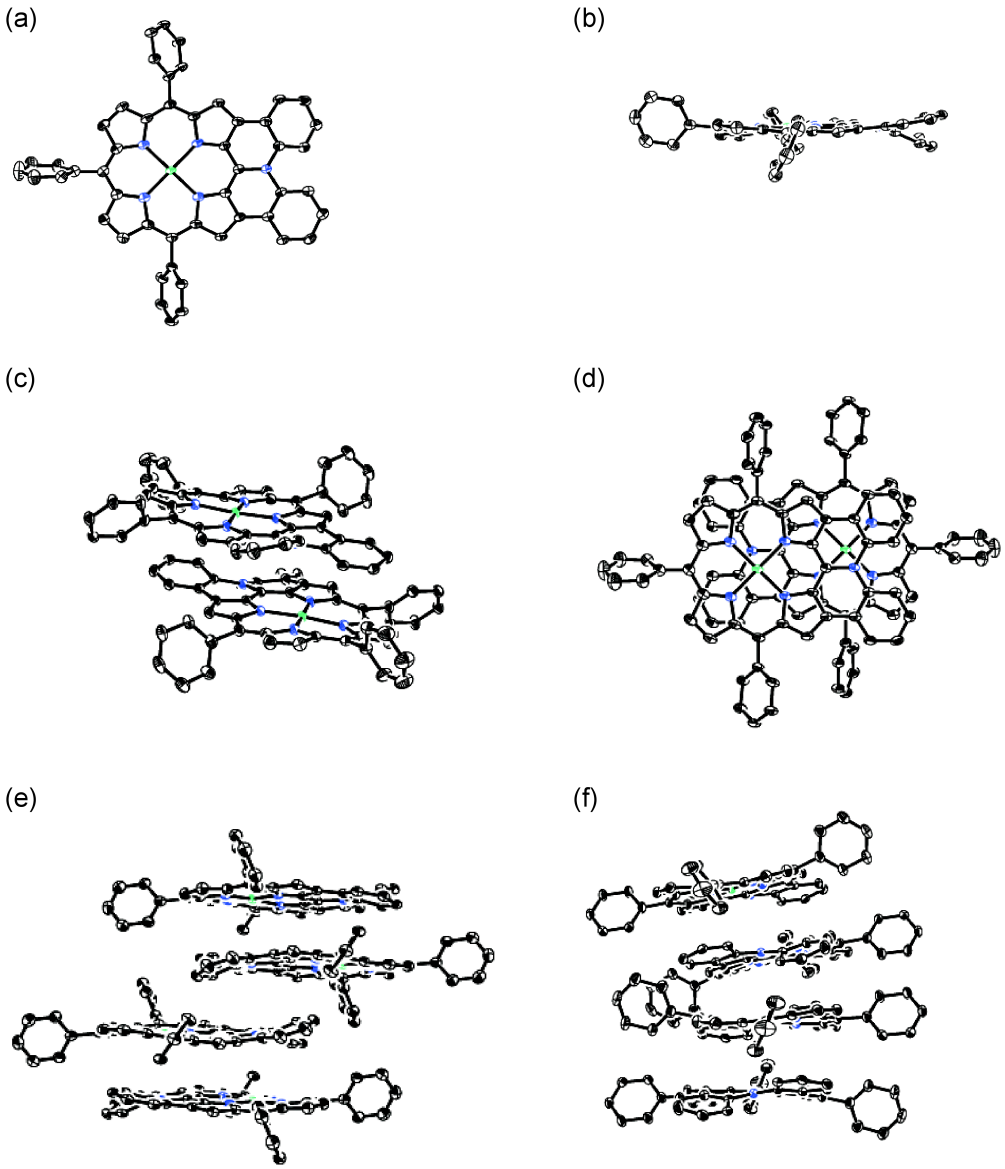

Figure S 50. X-Ray crystal structures of **10Ni**. (a) Top view and (b) side view of the single molecule. (c) Over view and (d) top view of the π-stacked dimer. (e,f) Side views of the packing structure. Thermal ellipsoids are shown at the 50% probability level. Solvent molecules, *tert*-butyl groups, and all hydrogen atoms are omitted for clarity.

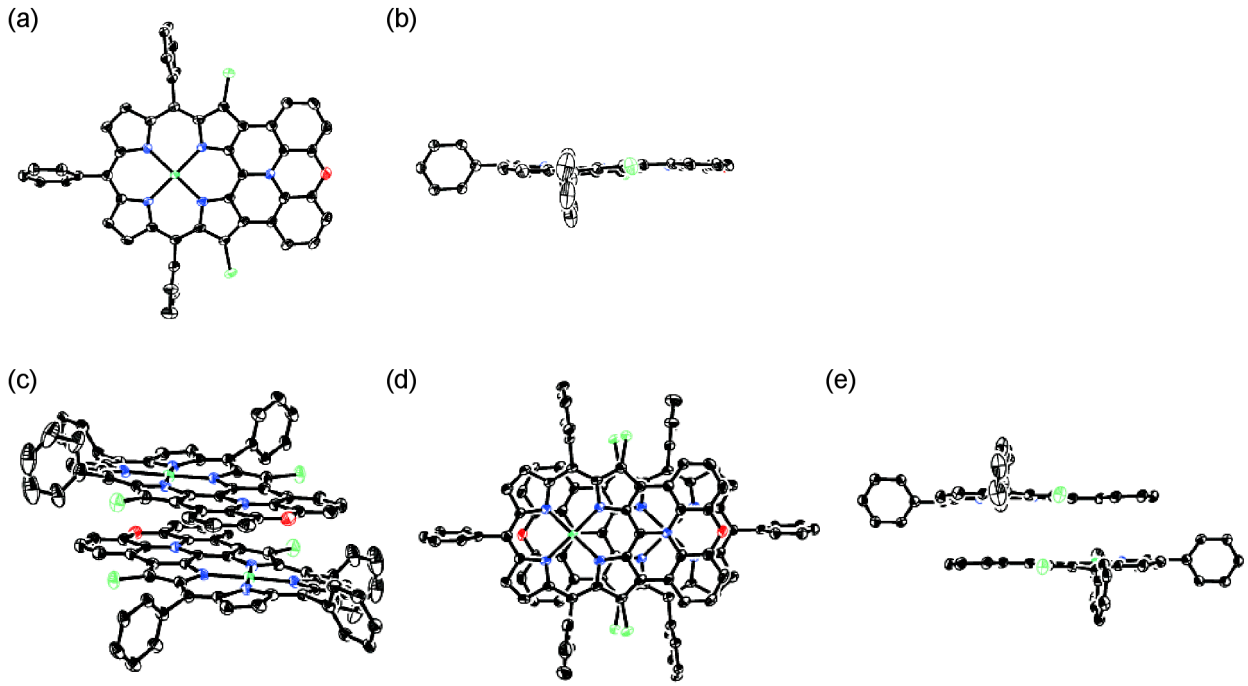

Figure S 51. X-Ray crystal structures of **13**. (a) Top view and (b) side view of the single molecule. (c) Over view, (d) top view, and (e) side view of the π-stacked dimer. Thermal ellipsoids are shown at the 50% probability level. Solvent molecules, *tert*-butyl groups, and all hydrogen atoms are omitted for clarity.

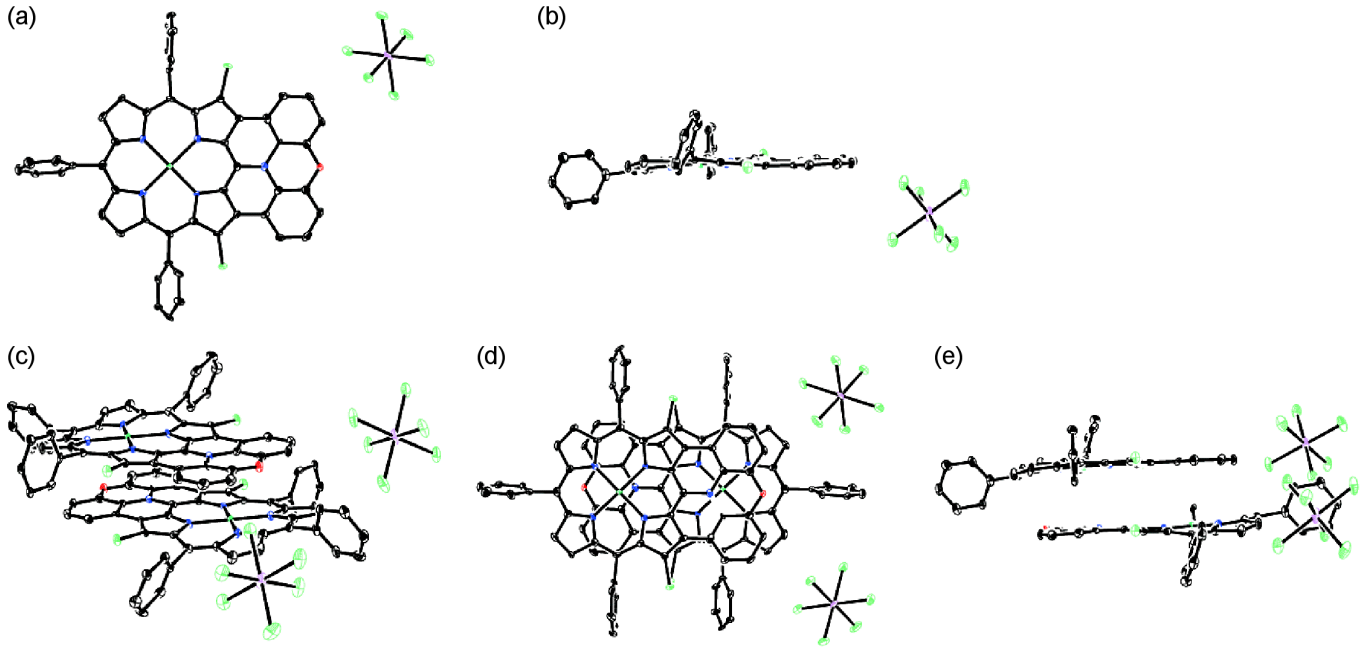

Figure S 52. X-Ray crystal structures of **[13]**$^{+}$. (a) Top view and (b) side view of the single molecule. (c) Over view, (d) top view, and (e) side view of the π-stacked dimer. Thermal ellipsoids are shown at the 50% probability level. Solvent molecules, *tert*-butyl groups, and all hydrogen atoms are omitted for clarity.

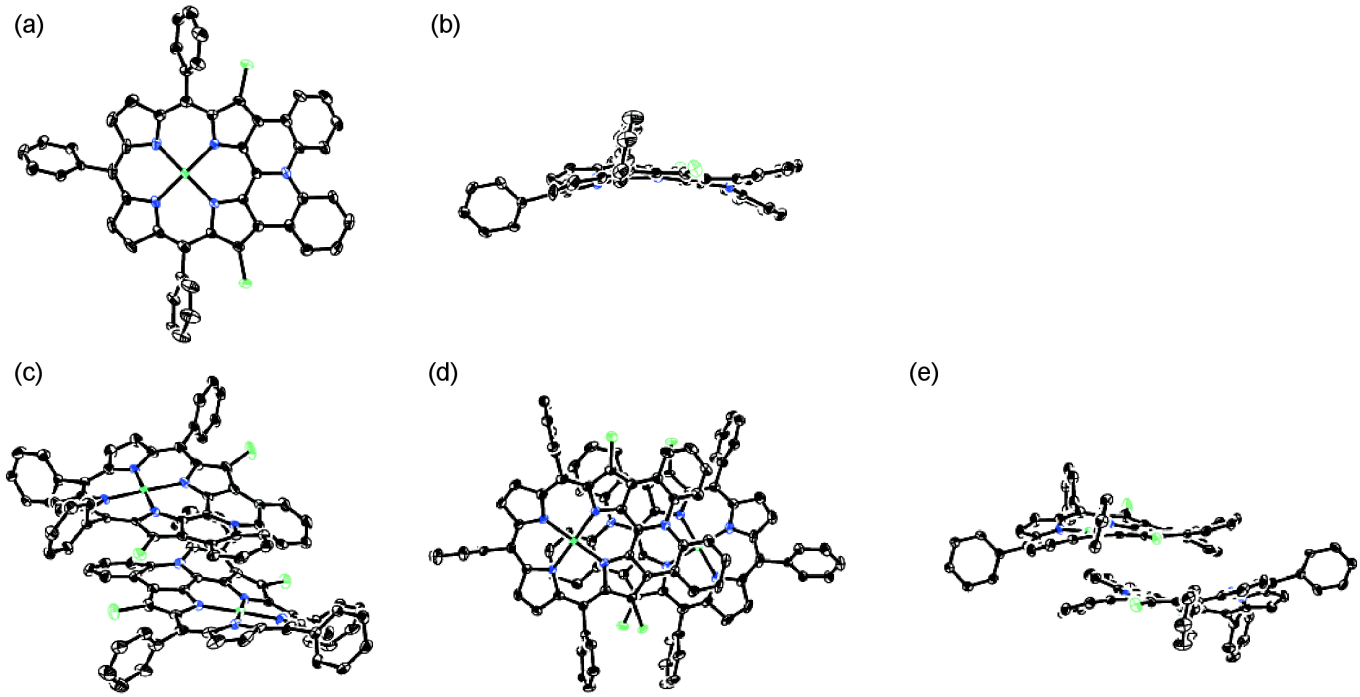

Figure S 53. X-Ray crystal structures of **14**. (a) Top view and (b) side view of the single molecule. (c) Over view, (d) top view, and (e) side view of the π-stacked dimer. Thermal ellipsoids are shown at the 50% probability level. Solvent molecules, *tert*-butyl groups, and all hydrogen atoms are omitted for clarity.

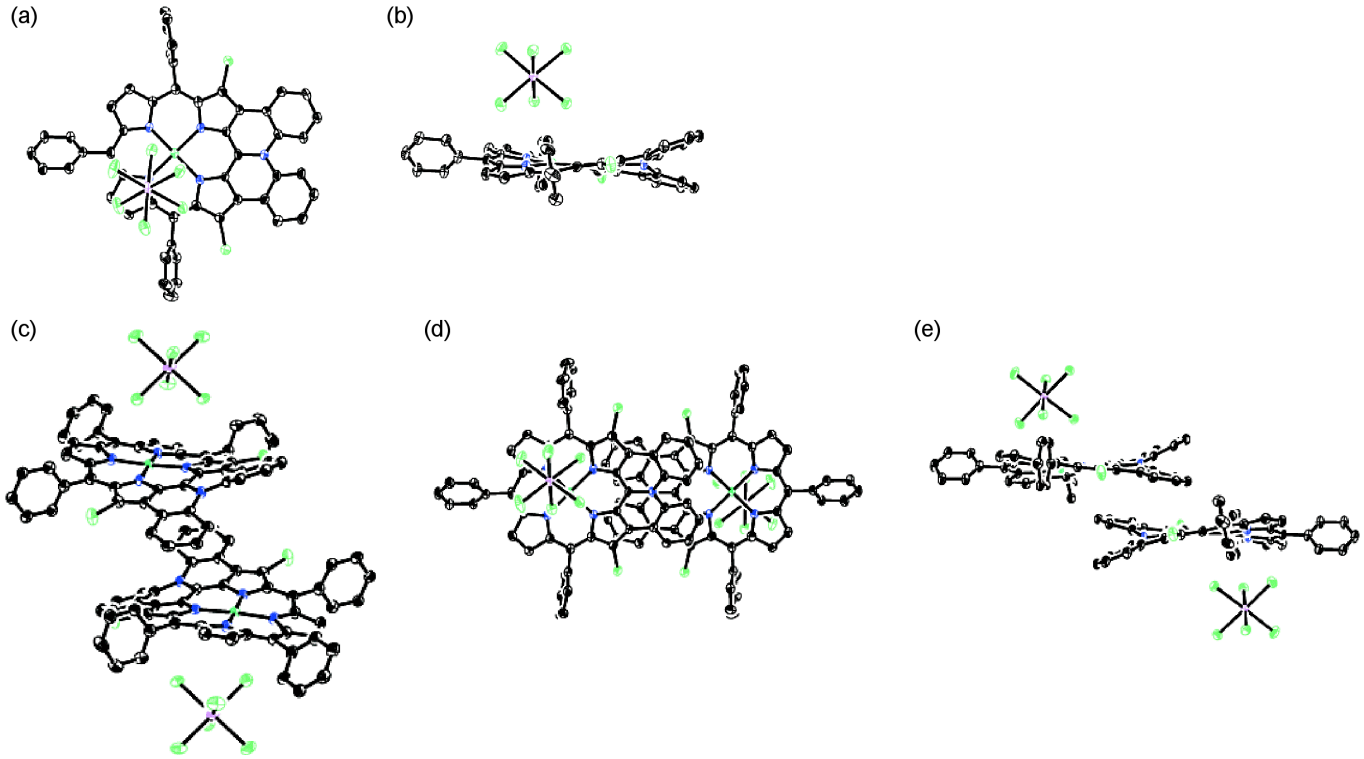

Figure S 54. X-Ray crystal structures of **[14]**$^{+}$. (a) Top view and (b) side view of the single molecule. (c) Over view, (d) top view, and (e) side view of the π-stacked dimer. Thermal ellipsoids are shown at the 30% probability level. Solvent molecules, *tert*-butyl groups, and all hydrogen atoms are omitted for clarity.

Table S 1. Crystal data and structure refinements for **9**, **4Ni**, and **10Ni**.

Compound	**9**	**4Ni**	**10Ni**
Empirical Formula	$C_{74}H_{77}N_5NiO$, 0.3(C_2H_5OH), 0.41 ($CHCl_3$)	$C_{74}H_{75}N_5NiO$, 1.5($C_6H_5CH_3$)	$C_{74}H_{77}N_5Ni$, $CHCl_3$, CH_3CN
Mw	1170.47	1243.27	1251.30
Crystal System	Triclinic	Monoclinic	Monoclinic
Space Group	*P*-1 (No. 2)	$P2_1/n$ (No. 14)	*C*2/*c* (No. 15)
a	12.375(7) Å	21.181(7) Å	36.653(7) Å
b	16.832(10) Å	10.751(4) Å	21.504(4) Å
c	18.491(10) Å	29.482(10) Å	17.115(3) Å
α	110.391(8)°	—	—
β	98.378(15)°	100.128(9)°	98.833(7)°
γ	106.7253(10)°	—	—
Volume	3325(3) $Å^3$	6609(4) $Å^3$	13330(4) $Å^3$
Z	2	4	8
Density (calcd.)	1.169 g/cm^3	1.250 g/cm^3	1.247 g/cm^3
Completeness	0.974	0.992	0.990
Goodness-of-fit	1.092	1.029	1.047
R_1 [$I>2\sigma(I)$]	0.0837	0.0714	0.0768
wR_2 (all data)	0.2483	0.2075	0.2444
Solvent System	$CHCl_3$/EtOH	toluene/MeOH	$CHCl_3$/MeCN
CCDC No.	1469156	1469155	1469154

Table S 2. Crystal data and structure refinements for **13**, **[13]**$^{+}$, **[14]** and **[14]**$^{+}$.

Compound	**13**	**[13]**$^{+}$	**14**	**[14]**$^{+}$
Empirical Formula	$2(C_{74}H_{73}Cl_2N_5NiO)$, $1.5(CHCl_3)$	$C_{74}H_{73}Cl_2N_5NiO$, $SbCl_6$, $2(C_6H_{14})$, CH_2Cl_2	$2(C_{74}H_{75}Cl_2N_5Ni)$, $1.5(CHCl_3)$, C_3H_7OH, H_2O	$C_{74}H_{75}Cl_2N_5Ni$, $SbCl_6$, $0.5(CH_2Cl_2)$
Mw	2535.01	1767.68	3143.91	1540.91
Crystal System	Triclinic	Tetragonal	Monoclinic	Monoclinic
Space Group	*P*-1 (No.2)	$I4_1/a$ (No. 88)	*C*2/*c* (No. 15)	$P2_1/n$ (No. 14)
a	18.141(3) Å	57.941(6) Å	72.720(9) Å	27.888(11) Å
b	20.0791(19) Å	57.941(6) Å	13.4081(16) Å	9.758(3) Å
c	20.299(2) Å	10.6631(12) Å	33.152(4) Å	29.846(11) Å
α	62.0374(10)°	—	—	—
β	79.030(16)°	—	102.869(4)°	113.508(6)°
γ	87.782(14)°	—	—	—
Volume	6400.6(14) Å^3	35798(8)	31513(7) Å^3	7448(5) Å^3
Z	2	16	8	4
Density (calcd.)	1.315 g/cm^3	1.312 g/cm^3	1.325 g/cm^3	1.374 g/cm^3
Completeness	0.970	0.964	0.964	0.986
Goodness-of-fit	1.045	1.079	1.064	1.004
R_1 [$I>2\sigma$ (I)]	0.0791	0.0992	0.0996	0.0826
wR_2 (all data)	0.2451	0.2692	0.2800	0.2363
Solvent System	$CHCl_3$/EtOH	CH_2Cl_2/hexane	$CHCl_3$/^{i}PrOH	CH_2Cl_2/heptane
CCDC No.	1469157	1469158	1469159	1469160

6. Electrochemical Properties

Cyclic voltammograms and differential pulse voltammograms were obtained under the following conditions; solvent: CH_2Cl_2, electrolyte: 0.1 M nBu$_4$NPF$_6$, working electrode: glassy carbon, counter electrode: Pt, reference electrode: Ag/AgClO$_4$, scan rate: 0.05 V/s (E > 0.27 V) and 0.50 V/s (E < 0.27 V).

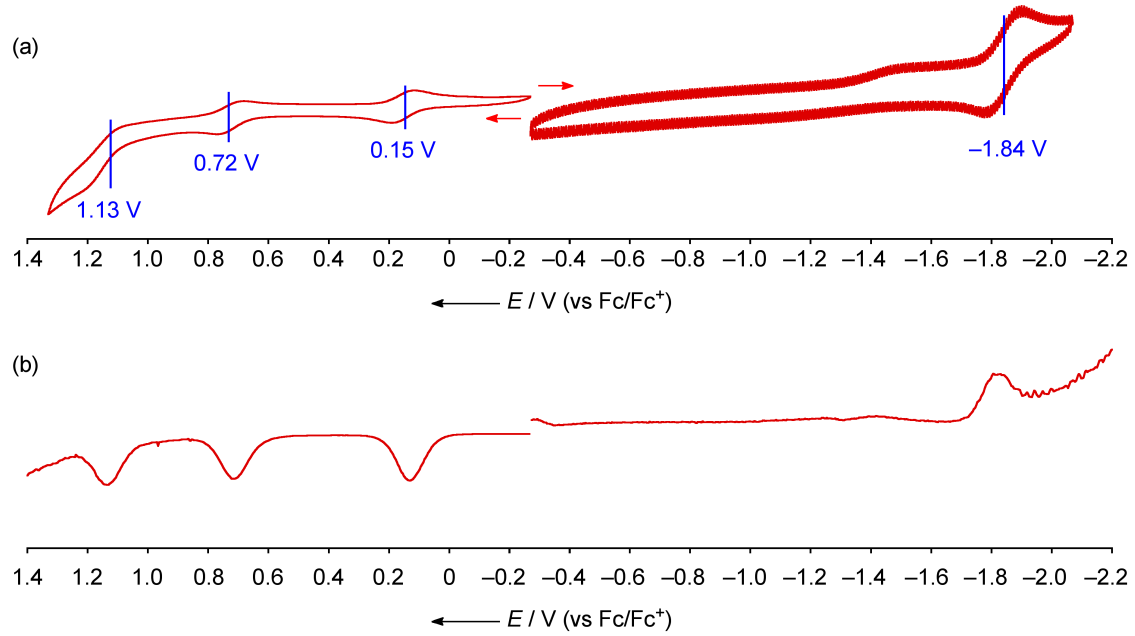

Figure S 55. (a) Cyclic voltammograms and (b) differential pulse voltammograms of **10Ni**.

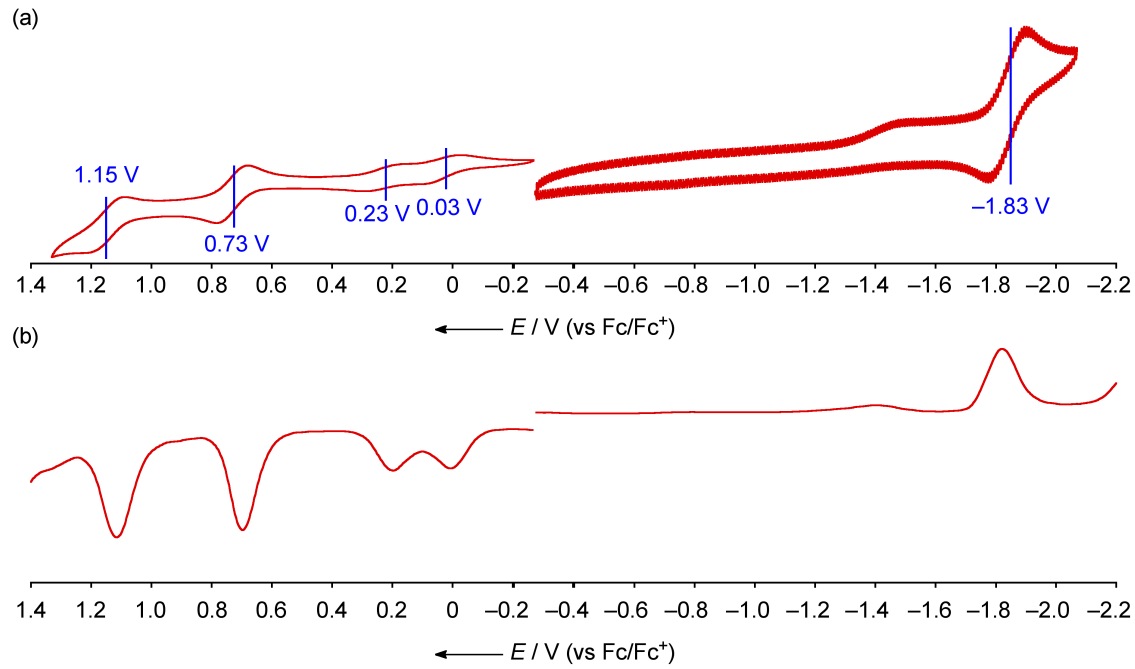

Figure S 56. (a) Cyclic voltammograms and (b) differential pulse voltammograms of **4Ni** at 2.2 mM.

7. ESR Spectra

ESR spectra for the toluene solution samples of **[13]**$^+$ and **[14]**$^+$ were measured by using JEOL JES-FA200 spectrometer at room temperature. Samples of **[13]**$^+$ and **[14]**$^+$ (0.049 and 0.047 mM in toluene, respectively) were degassed by freeze-pump-thaw cycles in quartz tube and sealed by frame. The observed ESR signals for were reproduced by a single gaussian signal without hyperfine structure of g = 2.0031 and 2.0029, respectively.

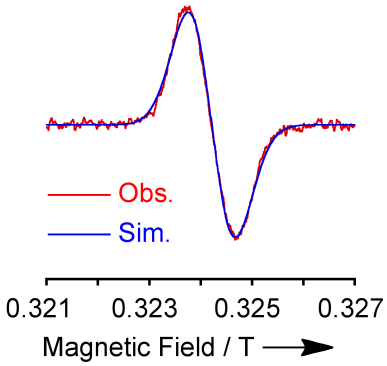

Figure S 57. Observed ESR spectrum of **[13]**$^+$ (0.049 mM in toluene) at room temperature (g = 2.0031).

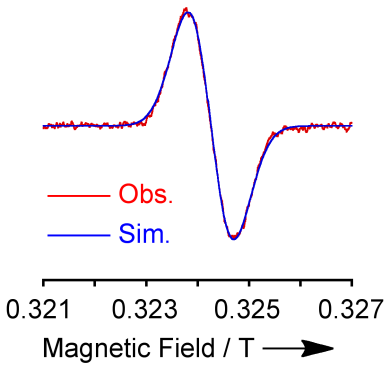

Figure S 58. Observed ESR spectrum of **[14]**$^+$ (0.047 mM in toluene) at room temperature (g = 2.0029).

8. Temperature Dependent Magnetic Susceptibility

Magnetic susceptibility was measured for the powder sample of **[13]**$^+$ and **[14]**$^+$ with the temperature range from 2 to 350 K at 0.5 T magnetic field by a Quantum Design MPMS-2S instrument.

The simulated χT values of **[13]**$^+$ were obtained by Bleaney–Bowers singlet-triplet model (Eq. 8) with fitted parameters of $f_1 = 0.50$, $f_2 = 0.15$, and $J_1/k_B = -30.4$ K.

$$\chi T = f_1 \frac{N_A g^2 \mu_B{}^2}{k_B[3 + \exp(-2J_1/k_B T)]} + f_2 \frac{N_A g^2 \mu_B{}^2}{2k_B} \quad (8)$$

The simulated χT values of **[14]**$^+$ were obtained by Bonner–Fisher model (Eq. 9, 10) with fitted parameters of $f = 0.94$ and $J_1/k_B = -1.6$ K.

$$\chi T = f \frac{N g^2 \mu_B{}^2}{k_B} \frac{0.25 + 0.14995x + 0.30094x^2}{1 + 1.9862x + 0.68854x^2 + 6.0626x^3} \quad (9)$$

$$x = \frac{|J_1|}{k_B T} \quad (10)$$

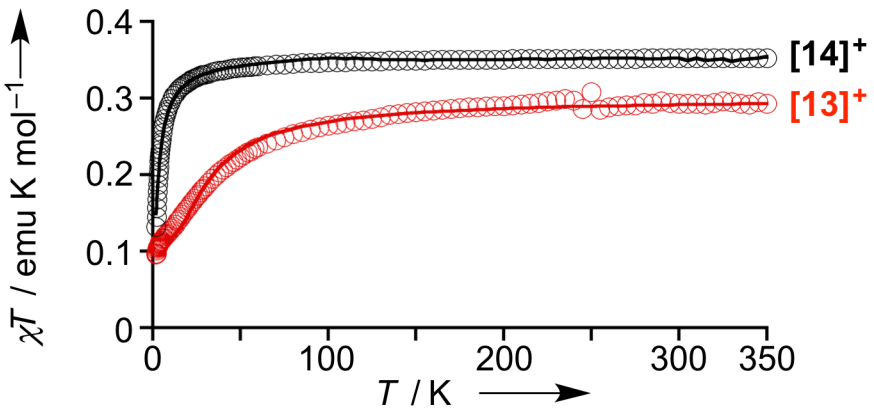

Figure S 59. Temperature dependent magnetic susceptibility of **[13]**$^+$ (red) and **[14]**$^+$ (black) by SQUID measurement. Circles: observed χT value. Solid line: simulated.

9. DFT Calculations

All calculations were carried out using the *Gaussian 09* program.[S3] The geometry was obtained from X-ray structures. The calculations of **4Ni** and **7** were performed by the density functional theory (DFT) method with restricted B3LYP (Becke's three-parameter hybrid exchange functionals and the Lee-Yang-Parr correlation functional)[S4] level, employing basis sets 6-31G(d) for C, H, O, and N and LANL2DZ for Ni. The calculation of **[6Ni]**$^+$ and **[13]**$^+$ was performed by DFT method with unrestricted B3LYP level, employing basis sets 6-31G(d) for C, H, O, N, and Cl and LANL2DZ for Ni. *tert*-Butyl groups were replaced with hydrogen atoms to simplify the calculation.

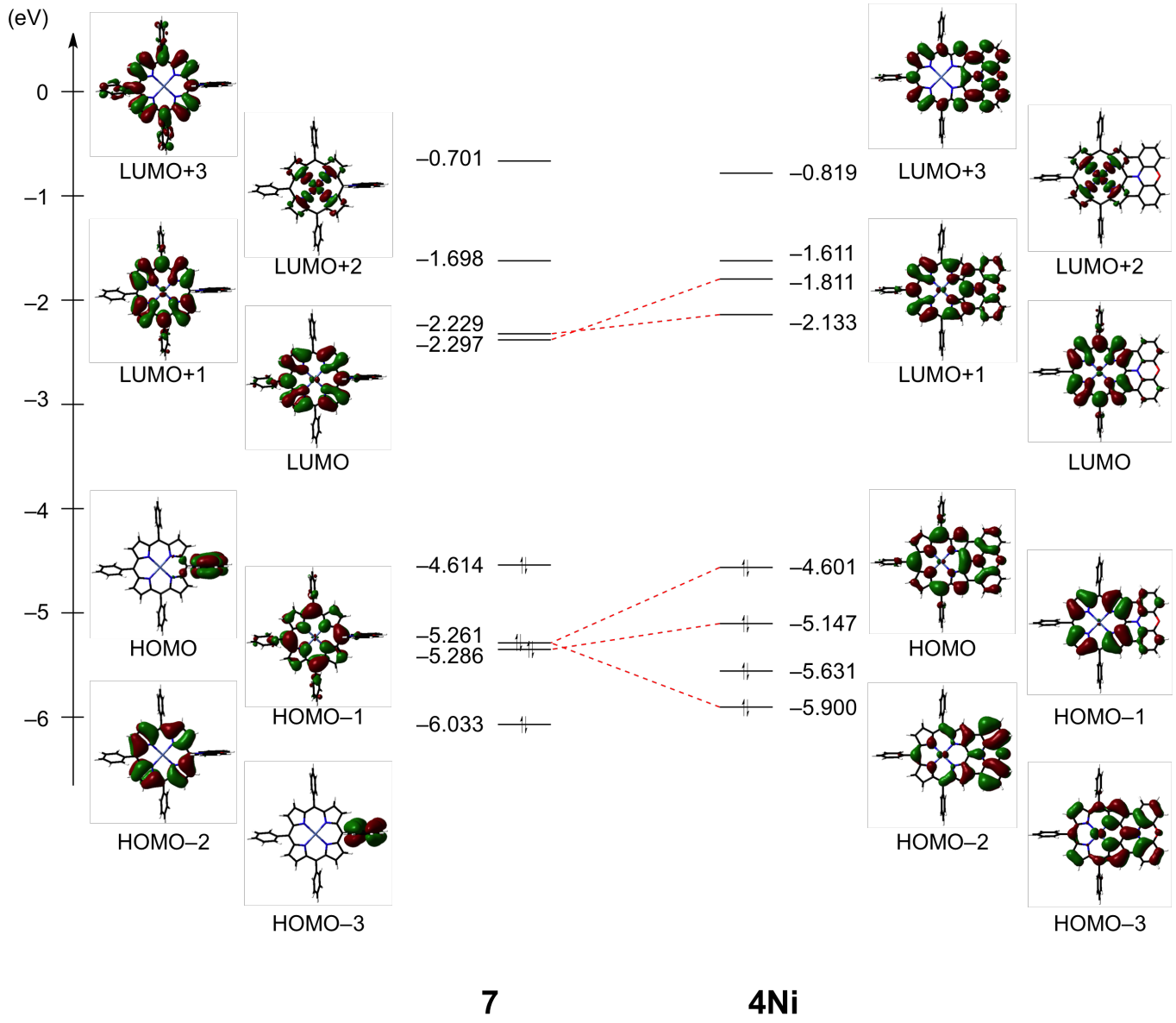

Figure S 60. Energy diagrams and Kohn-Sham orbital representations of **4Ni** and **7**.

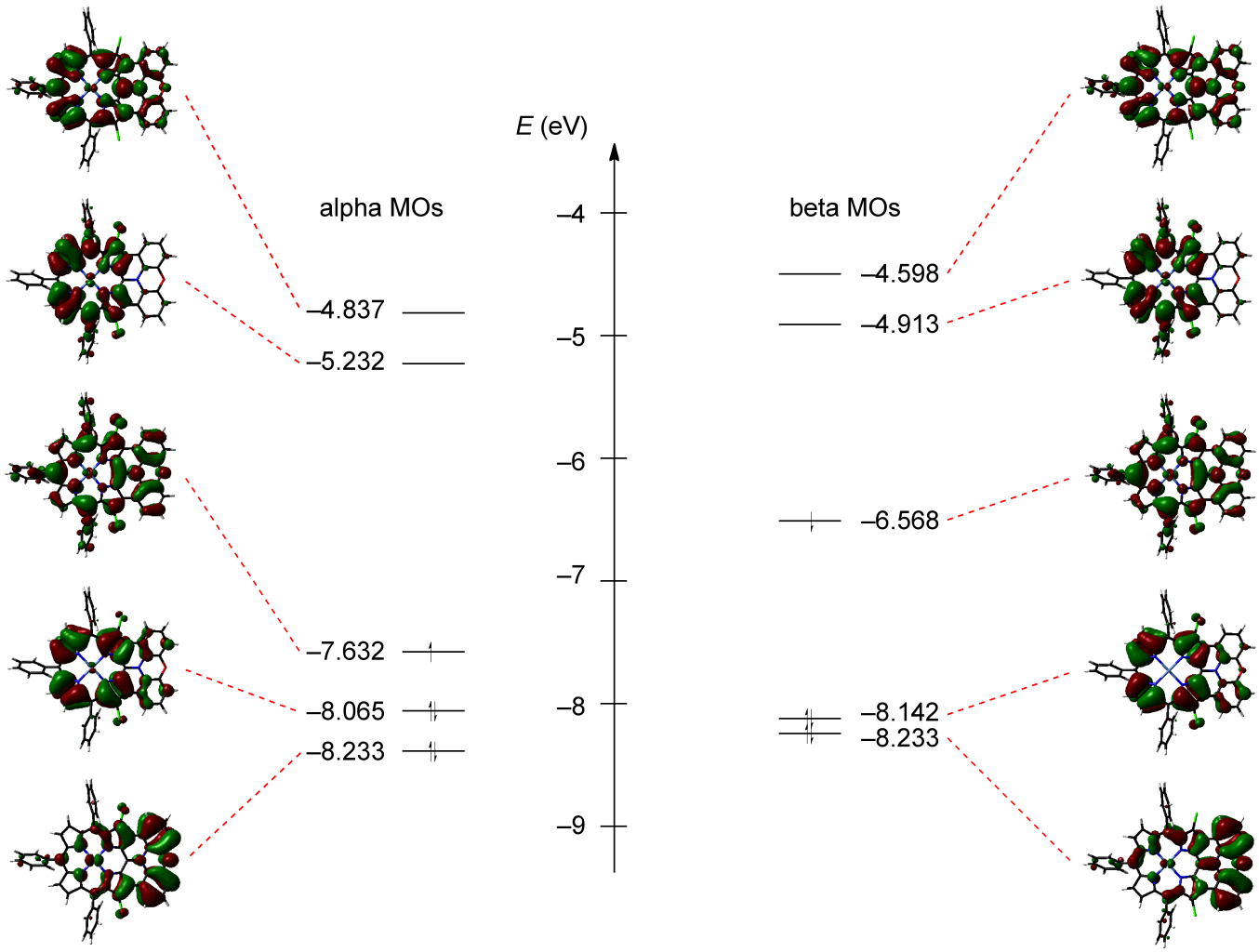

Figure S 61. Energy diagrams and Kohn-Sham orbital representations of **[13]**$^{+}$.

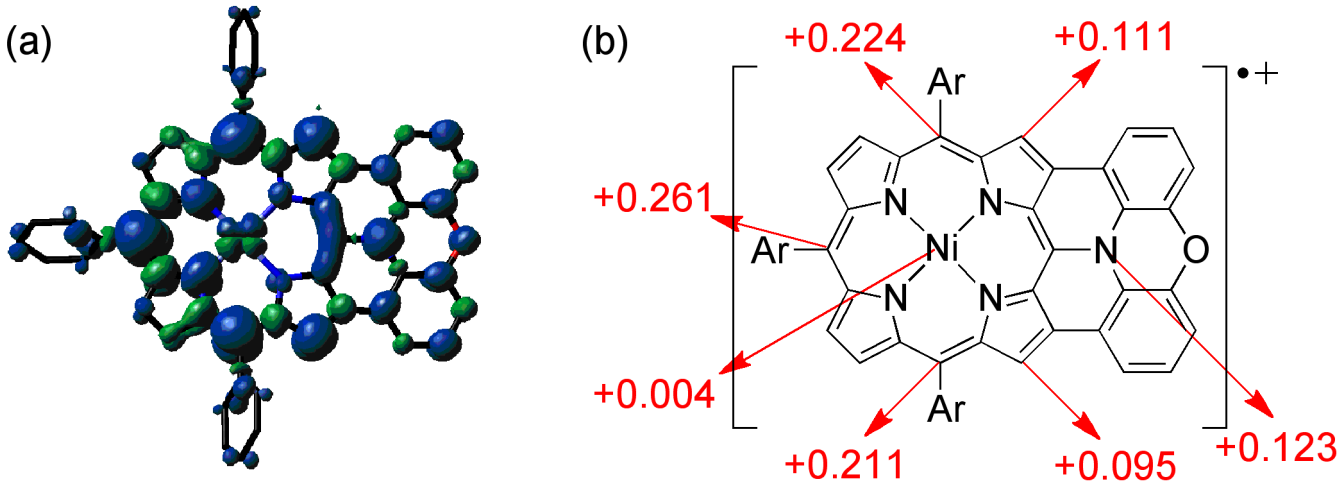

Figure S 62. (a) Spin density distribution and (b) selected values of **[4Ni]**$^{+}$ (isovalue: 0.001; the molecular geometry was optimized based on the X-ray crystal structure of **[13]**$^{+}$).

10. Fluorescence Decay and Time-resolved TA Spectra

The time-correlated single-photon-counting (TCSPC) system was used for fluorescence decay profiles.[S5] The transient absorption spectra were obtained by using home-made femtosecond time-resolved transient absorption (fs-TA) spectrometer. The spectrometer consists of an optical parametric amplifier (OPA; Palitra, Quantronix) pumped by a Ti:sapphire regenerative amplifier system (Integra-C, Quantronix) operating at 1 kHz repetition rate and an optical detection system.[S5]

Table S 3. Radiative and non-radiative rate constants of **10H$_2$**, **10Zn**, **4H$_2$**, and **4Zn**.

Compound	**10H$_2$**	**10Zn**	**4H$_2$**	**4Zn**
Radiative decay rate (k_r) [s^{-1}]	3.5 x 10^7	5.2 x 10^7	4.7 x 10^7	5.9 x 10^7
Non-radiative decay rate (k_{nr}) [s^{-1}]	1.7 x 10^8	3.5 x 10^8	1.3 x 10^8	3.1 x 10^8

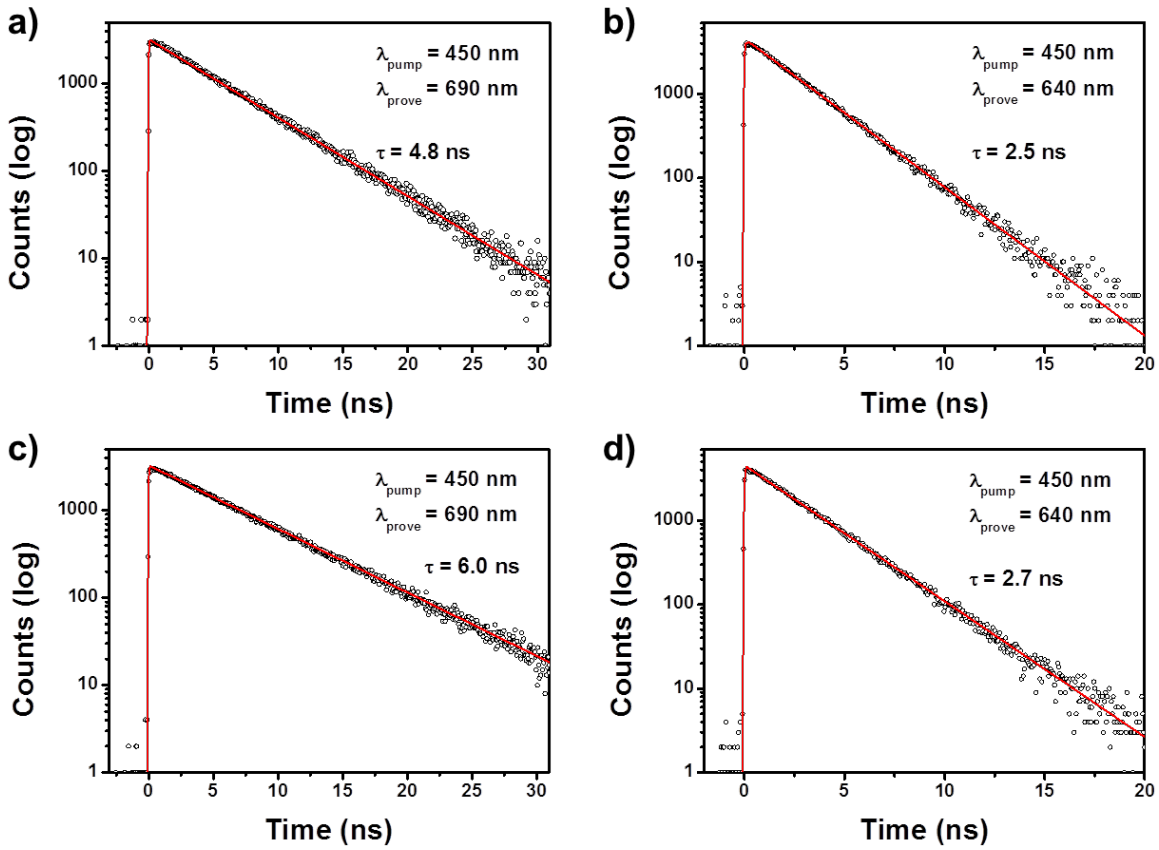

Figure S 63. Time-correlated single photon counting (TSCPC) decay curves of a) **10H$_2$**, b) **10Zn**, c) **4H$_2$**, and d) **4Zn**.

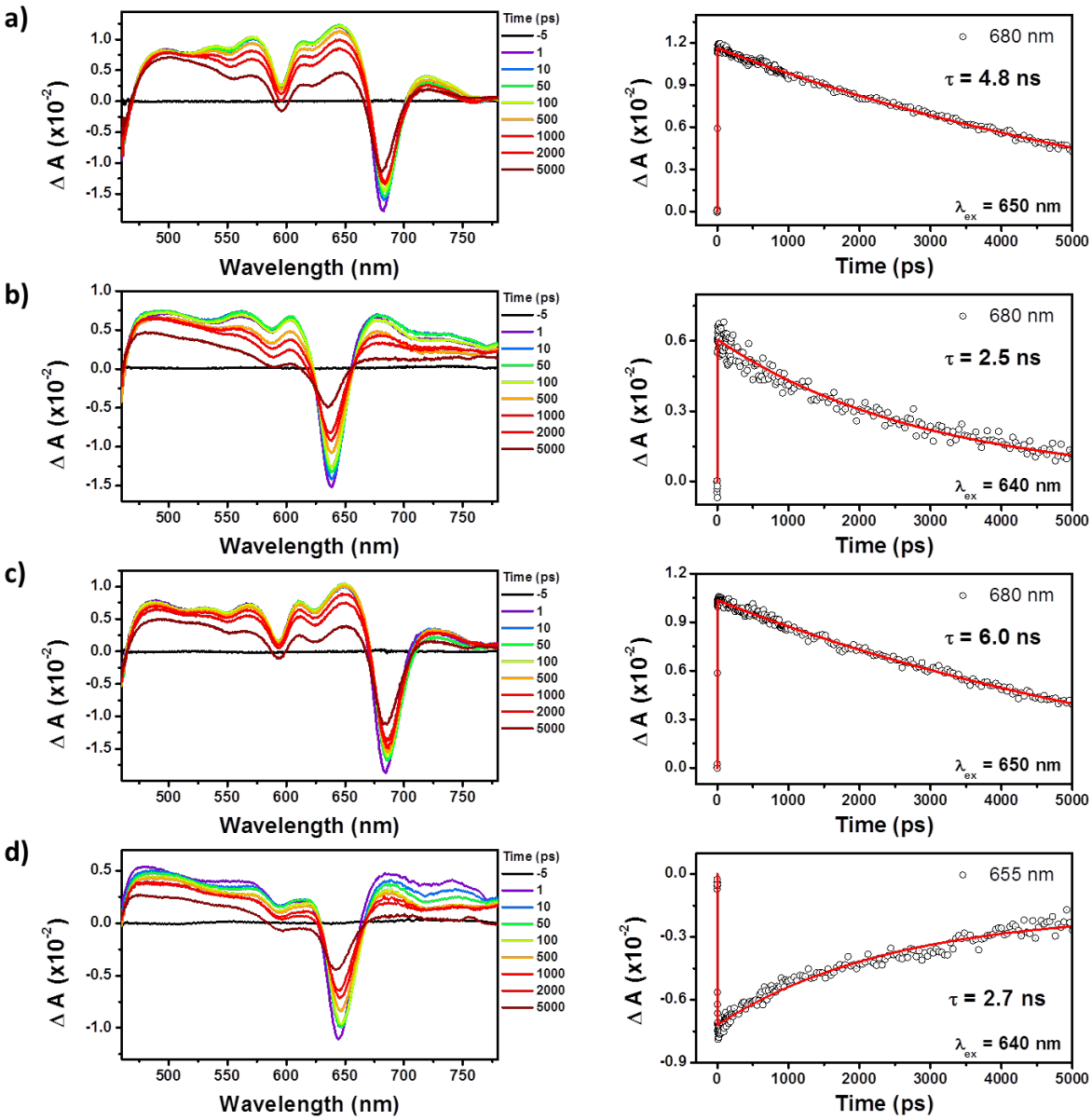

Figure S 64. TA spectra (left) and decay profiles (right) of a) **10H**$_2$, b) **10Zn**, c) **4H**$_2$, and d) **4Zn** in CH_2Cl_2 with photoexcitation at 685 nm for **4H**$_2$ and **10H**$_2$, and 649 nm for **4Zn** and **10Zn**.

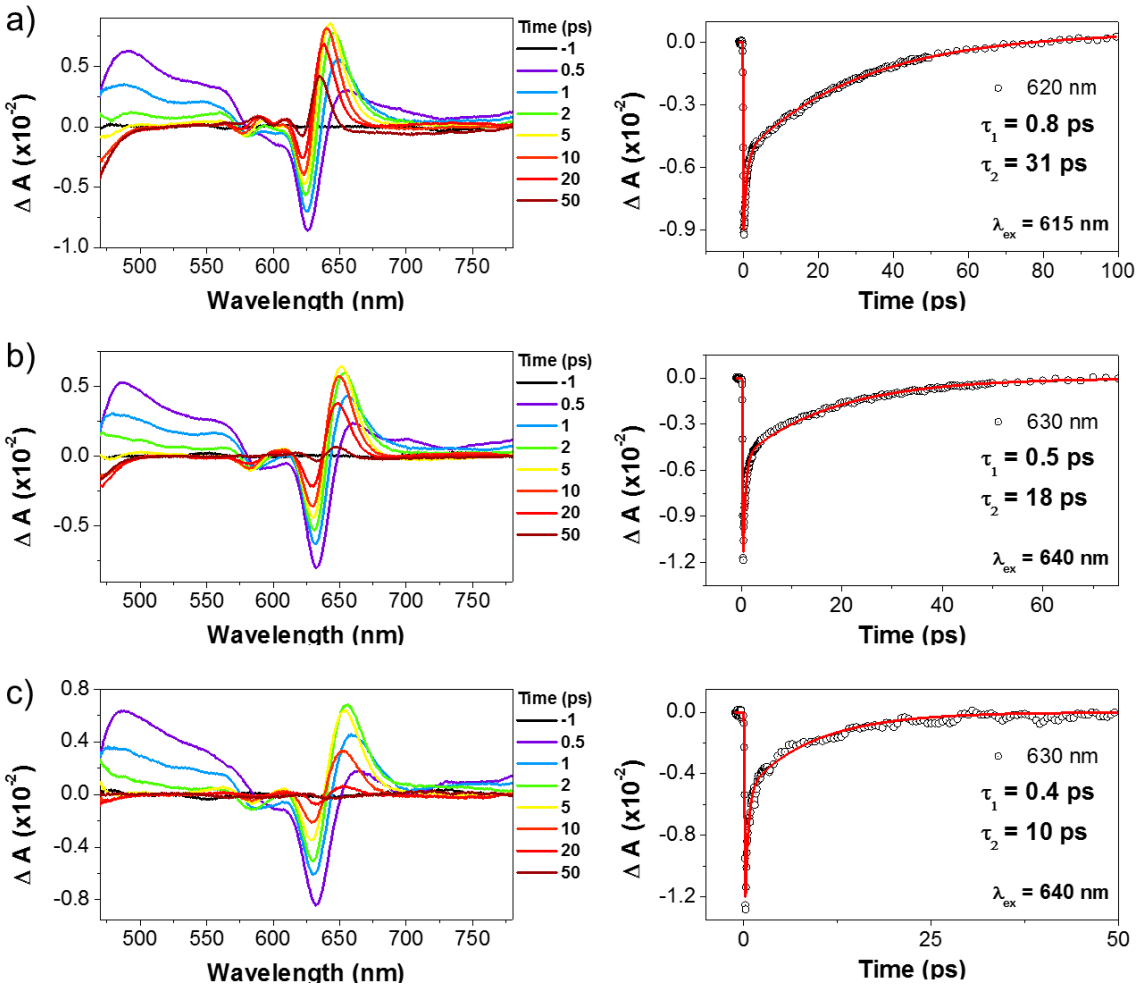

Figure S 65. TA spectra (left) and decay profiles (right) of **13** in a) methyl cyclohexane, b) toluene, and c) CH_2Cl_2 with photoexcitation at 615, 640, and 640 nm, respectively.

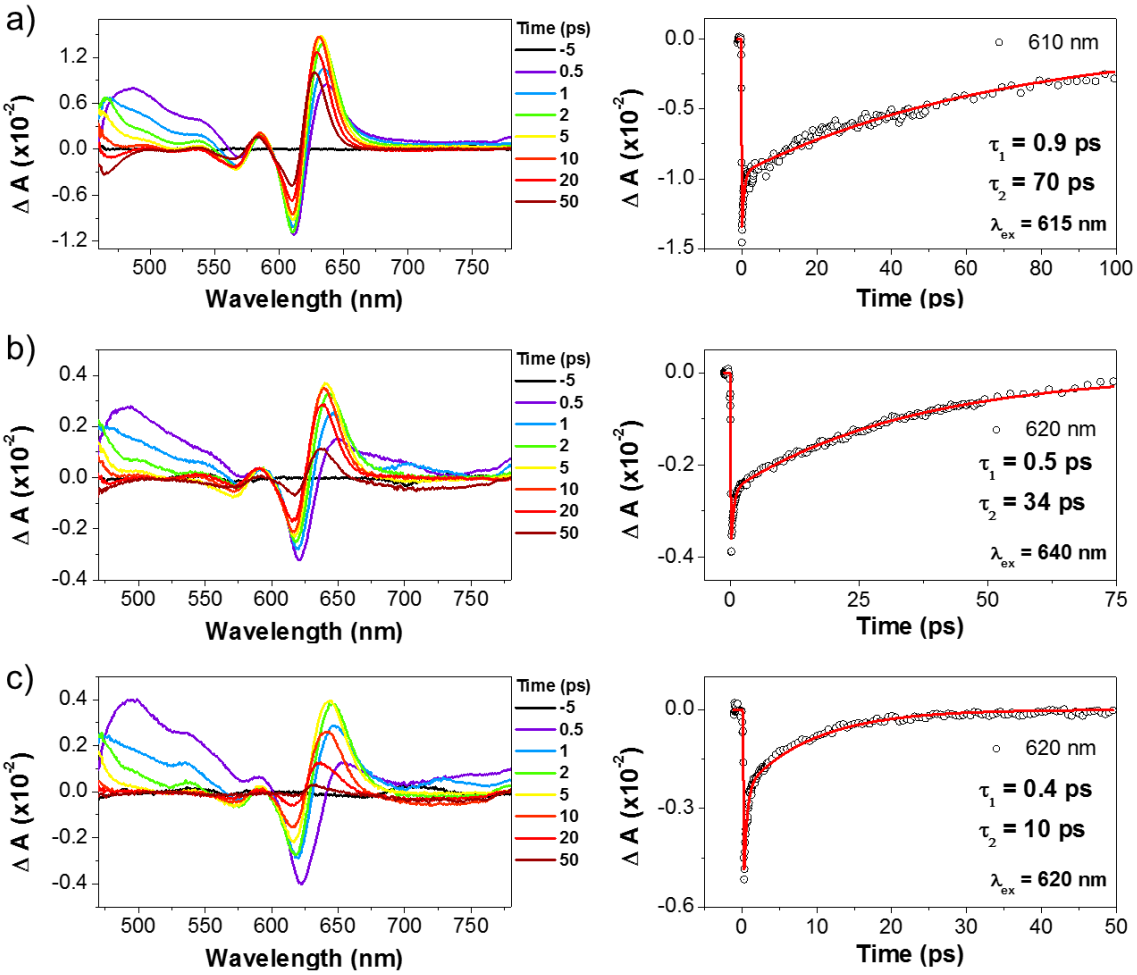

Figure S 66. TA spectra (left) and decay profiles (right) of **14** in a) methyl cyclohexane, b) toluene, and c) CH_2Cl_2 with photoexcitation at 615, 640, and 620 nm, respectively.

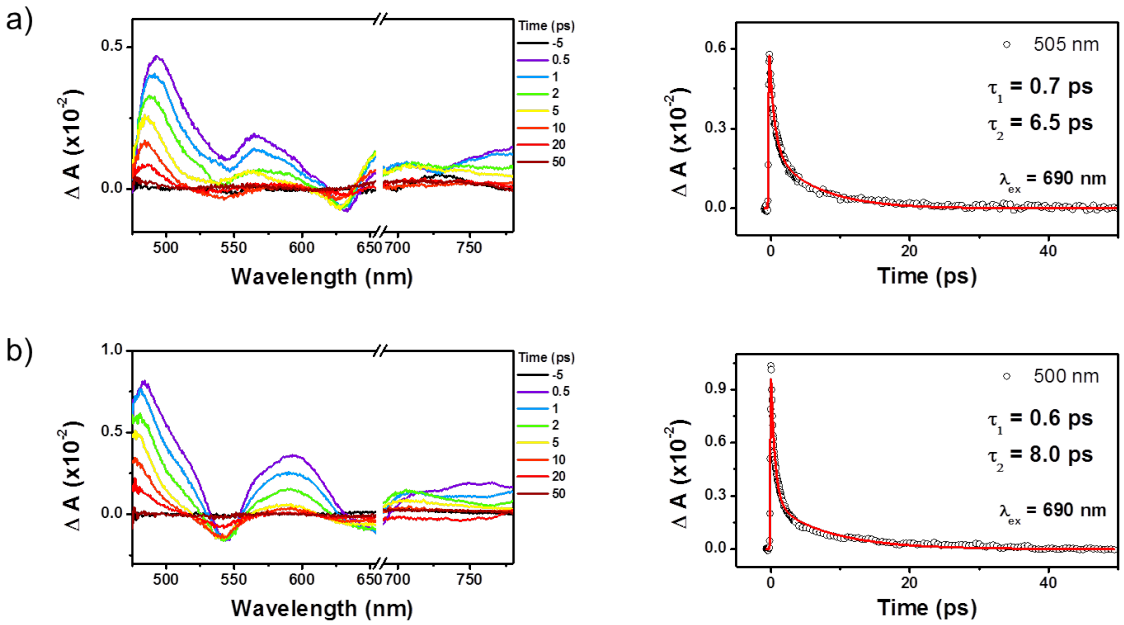

Figure S 67. TA spectra (left) and decay profiles (right) of a) **[13]**$^+$ and b) **[14]**$^+$ in toluene with photoexcitation at 690 nm.

11. Z-Scan Curves in TPA Measurements

The two-photon absorption (TPA) cross-section were measured using the open-aperture Z-scan method with 130 fs pulses from an optical parametric amplifier (Light Conversion, TOPAS) operating at a 2 kHz repetition rate using a Ti:sapphire regenerative amplifier system (Spectra-Physics, Hurricane).[S6]

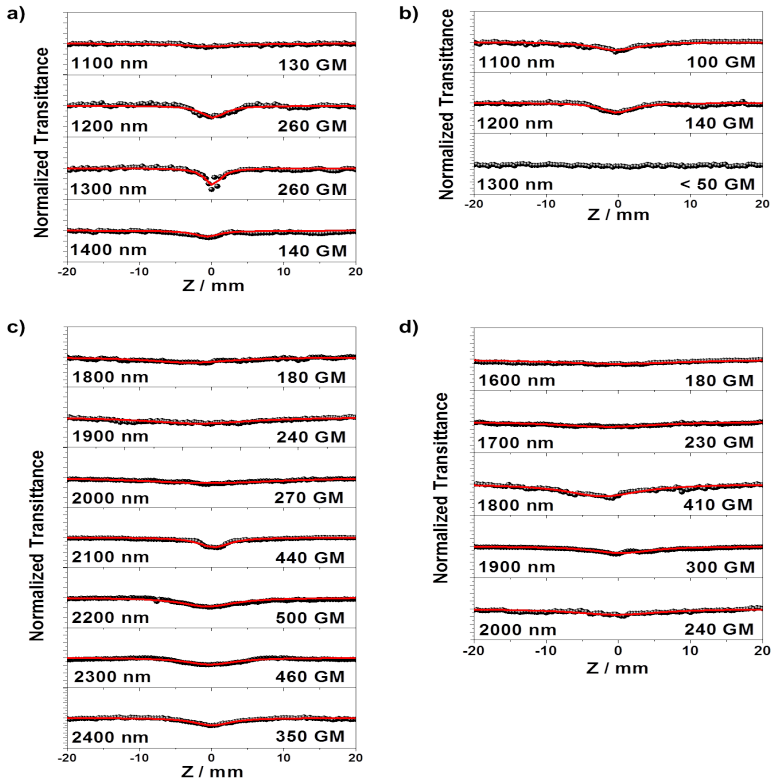

Figure S 68. Z-scan curves of a) **13**, b) **14**, c) **[13]**$^{+}$, and d) **[14]**$^{+}$ in toluene.

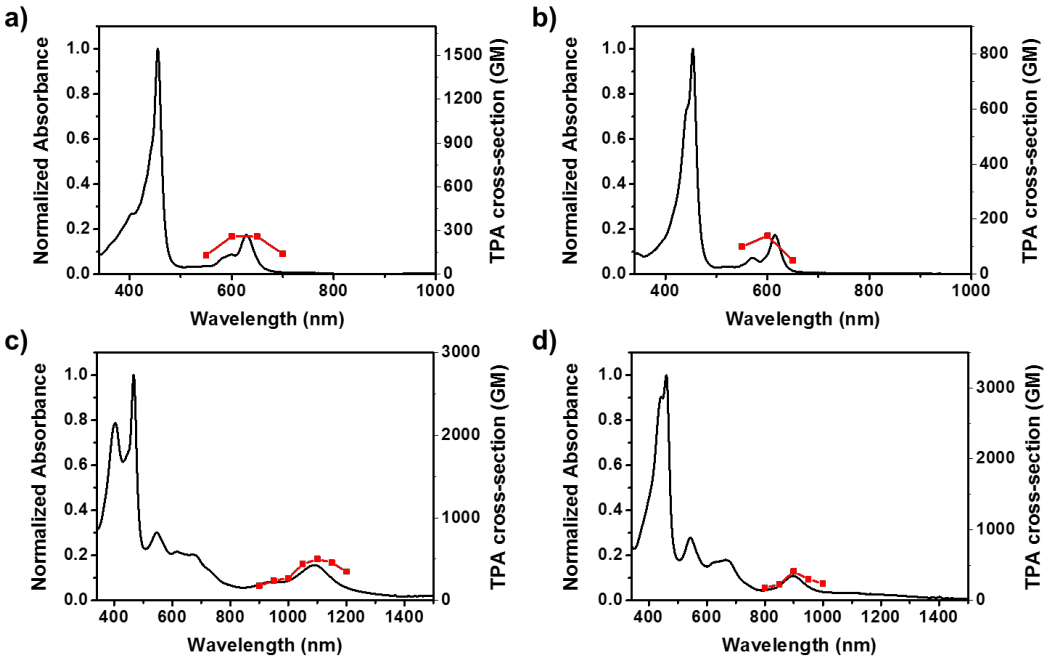

Figure S 69. One photon absorption (black solid line and left vertical axis) and two photon absorption (red line connecting red square symbols and right vertical axis) of a) **13**, b) **14**, c) **[13]**$^{+}$, and d) **[14]**$^{+}$

12. References

[S1] SHELXL-97 program for refinement of crystal structures from diffraction data, University of Goettingen, Goettingen (Germany); G. Sheldrick, T. Schneider, *Methods Enzymol.* **1997**, *277*, 319. SIR-97 program for solution of crystal structures from diffraction data: A. Altomare, M. C. Burla, M. Camalli, G. L. Cascarano, C. Giacovazzo, A. Guagliardi, A. G. G. Moliterni, G. Polidori, R. Spagna, *J. Appl. Cryst*. **1999**, *32*, 115-119.

[S2] a) I. Horman, B. Dreux, *Helv. Chim. Acta* **1984**, *67*, 754; b) C.-J. Wallentin, T. Wixe, O. F. Wendt, K.-E. Bergquist, K. Wärnmark, *Chem. Eur. J.* **2010**, *16*, 3994.

[S3] G aussian 09, Revision A.02, M. J. Frisch, G. W. Trucks, H. B. Schlegel, G. E. Scuseria, M. A. Robb, J. R. Cheeseman, G. Scalmani, V. Barone, B. Mennucci, G. A. Petersson, H. Nakatsuji, M. Caricato, X. Li, H. P. Hratchian, A. F. Izmaylov, J. Bloino, G. Zheng, J. L. Sonnenberg, M. Hada, M. Ehara, K. Toyota, R. Fukuda, J. Hasegawa, M. Ishida, T. Nakajima, Y. Honda, O. Kitao, H. Nakai, T. Vreven, J. A. Montgomery, Jr., J. E. Peralta, F. Ogliaro, M. Bearpark, J. J. Heyd, E. Brothers, K. N. Kudin, V. N. Staroverov, R. Kobayashi, J. Normand, K. Raghavachari, A. Rendell, J. C. Burant, S. S. Iyengar, J. Tomasi, M. Cossi, N. Rega, J. M. Millam, M. Klene, J. E. Knox, J. B. Cross, V. Bakken, C. Adamo, J. Jaramillo, R. Gomperts, R. E. Stratmann, O. Yazyev, A. J. Austin, R. Cammi, C. Pomelli, J. W. Ochterski, R. L. Martin, K. Morokuma, V. G. Zakrzewski, G. A. Voth, P. Salvador, J. J. Dannenberg, S. Dapprich, A. D. Daniels, O. Farkas, J. B. Foresman, J. V. Ortiz, J. Cioslowski, and D. J. Fox, Gaussian, Inc.: Wallingford, CT, 2009.

[S4] a) A. D. Becke, *J. Chem. Phys.* **1993**, *98*, 1372; b) C. Lee, W. Yang, R. G. Parr, *Phys. Rev. B* **1998**, *37*, 785.

[S5] D. Shimizu, J. Oh, K. Furukawa, D. Kim, A. Osuka, *Angew. Chemie Int. Ed.* **2015**, *54*, 6613.

[S6] P. Kim, S. Ham, J. Oh, H. Uoyama, H. Watanabe, K. Tagawa, H. Uno, D. Kim, *Phys. Chem. Chem. Phys.* **2013**, *15*, 10612.